Phase Change Activation and Characterization of Spray-Deposited Poly(vinylidene) Fluoride Piezoelectric Thin Films

By

Miranda Tiffany Riosbaas

B.S. (University of Michigan, Ann Arbor) 2012

THESIS

Submitted in partial satisfaction of the requirements for the degree of

MASTER OF SCIENCE

in

Mechanical and Aeronautical Engineering

in the

OFFICE OF GRADUATE STUDIES

of the

UNIVERSITY OF CALIFORNIA

DAVIS

Approved:

_____

Kenneth J. Loh, Co-Chair

_____

Bryan R. Loyola, Co-Chair

_____

David A. Horsley

Committee in Charge

2014

Acknowledgements

Foremost, I would like to express my sincere gratitude to my advisors Professor Ken Loh of the University of California at Davis and Dr. Bryan Loyola of Sandia National Laboratories. Without the help and guidance offered over the last year this thesis would not have been possible. The examples of hard work, dedication, and motivation that have been presented to me have been nothing less than inspirational. To Bryan, I am forever indebted to you for letting me explore the world of a national lab and for allowing my research to turn in ways we would not have initially predicted. Your constant patience and support made this an unforgettable experience.

To my Mom, thank you for always letting me know that I could achieve anything that I set my mind to. To my Dad, thank you for teaching me the definition of hard work and for never letting me learn to sit and relax. I would not have succeeded in college without the lessons that you both taught me throughout my younger years. To Adriana, thank you for being such an inspirational and stable figure in my life. Your support and strength has been unwavering and there are no words to describe how truly thankful I am for the role you have played in my success thus far. To Dustin, thank you for always giving me a good laugh with your witty jokes. To my brother and sister, Jeremy and Julia, you have motivated me more than you will ever know. I look to both of you for light and cheer when I am overwhelmed and you never fail to provide me with laughter even in the most stressful of situations. To all of my siblings: Josh, Benny, Julia, Gerardo, Marni, and Matthew, thank you for providing invaluable quality time when I needed to step away from my responsibilities and take a moment to enjoy family. To my dear husband David, you have been my shining star throughout and have provided nothing but patience, laughter, guidance, and support through the journey of my college studies. Your selfless nature has been phenomenal and I am so thankful to have you by my side in our lifelong journey. To DJ, my little boy, your smile and presence never cease to lighten my mood at the end of a tough day. I will forever remember the grin and open arms that awaited me when walking through the door after a long day of research. And last but not least, thank you to my friends; Virginia, Hailey, Gianna, Brad, Chandler, and Yushi for providing life and technical support throughout my entire college career.

This material was based upon work supported by the National Science Foundation (NSF) Graduate Research Fellowship Program (GFRP) under Grant No. DGE-1148897. Any opinion, findings, and conclusions or recommendations expressed in this material are those of the authors(s) and do not necessarily reflect the views of NSF.

Abstract

Structural safety and integrity continues to be an issue of utmost concern in our world today. Existing infrastructures in civil, commercial, and military applications are beginning to see issues associated with age and environmental conditions. In addition, new materials are being put to service that are not yet fully characterized and understood when it comes to long term behavior. In order to assess the structural health of both old and new materials, it is necessary to implement a technique for monitoring wear and tear. Current methods that are being used today typically depend on visual inspection techniques or handheld instruments. These methods are not always ideal for large structures as they become very tedious leading to a substantial amount of both time and money spent. More recently, composite materials have been introduced into applications that can benefit from high strength-to-weight ratio materials. However, the use of more complex materials (such as composites) leads to a high demand of structural health monitoring techniques, since the damage is often internal and not visible to the naked eye.

The work performed in this thesis examines the methods that can be used for phase change activation and characterization of sprayable polyvinylidene fluoride (PVDF) thin films in order to exploit their piezoelectric characteristics for sensing applications. PVDF is widely accepted to exist in four phases: alpha, beta, gamma, and delta. Alpha phase PVDF is produced directly from the melt and exhibits no piezoelectric properties. The activation or transition from alpha phase to some combination of beta and/or gamma phase PVDF leads to a polarizable piezoelectric thin film to be used in sensing applications. The work herein presents the methods used to activate phase change in PVDF, such as mechanical stretching, annealing, and chemical composition, to be able to implement PVDF as an impact detection sensor. The results and analysis provided in this thesis will present the possibilities of spray-deposited PVDF thin films in both small-scale and large-scale sensing applications that can be applied to both simple and complex geometries.

Table of Contents

Chapter 1: Introduction

1.1 Current Infrastructure and Motivation

As the world continues to advance technologically and at a rapid rate, the infrastructures in our community continue to grow more complex in areas of both transportation and defense, among others. Currently, engineers are facing overwhelming challenges in developing new methods and ideas to create more reliable structures, all while maintaining safety of existing structures. This is applicable to current roadways, bridges, dams, aircraft, drinking water systems, etc. The estimated investment into the current infrastructure today is $3.6 trillion by the year 2020 [1]. Every four years, the American Society of Civil Engineers (ASCE) releases a report card for the infrastructure of America that shows the current condition of the existing infrastructure and their structural integrity. The United States is graded on aviation, bridges, dams, drinking water, and energy. For the 2013 release of the report card, America's graded average was calculated overall as a D+ [1]. More specifically, the aviation industry was graded at a D and bridges were given a C+. The significance of these grades are explained thoroughly where a C is described as mediocre and requiring some form of attention, and a D is described as poor and a risk to society. This is unfortunate as our population and technological needs continue to grow. An alarming statistic from the ASCE states that 12% of the bridges in California alone are considered to be structurally deficient, and another 16.8% of bridges are considered to be functionally obsolete [1].

In addition, the aerospace industry spends millions of dollars each year on maintenance across the commercial and military sectors. Specifically, the F-35 Joint Strike Fighter program will cost an estimated $1.1 trillion for maintenance over the lifetime of the program [2]. Within the aerospace industry, composite materials are being used in higher weight percentages for increased performance and reduced maintenance costs. For example, the Boeing 787 put into operation in 2011 was promised to provide less monitoring and maintenance due to the incorporation of composites by 50 % by weight [3]. According to Boeing, the long term behavior of the composite structures being incorporated into their airplane applications should lead to lower maintenance times. For example, the Boeing 777 composite tail is 25 % larger than the Boeing 767 aluminum tail yet requires 35 % fewer scheduled

maintenance labor hours due to the reduced risk of corrosion and fatigue of composites. However, these materials have vastly different damage characteristics than traditional monolithic metals. The unfamiliarity of these different damage characteristics has undoubtedly contributed to hesitations of composite use from the general population. Although current monitoring techniques and requirements are supposed to be reduced for composite structures, more complex requirements for safety testing *prior* to use have been implemented [4].

The current state of both civil and aviation structures supports the need for a means of structural monitoring to evaluate the integrity of a structure. This can be done by implementing structural health monitoring (SHM) techniques that will provide data in regards to the safety of the structure and if/when it may be completely compromised. In the SHM field, methods such as strain gages [5-8], optical fiber-based sensors [9-15], acoustic emission and ultrasonic based sensors [16-22], electrical-based sensors [23], and piezoelectric sensors [17, 18, 24] have been researched. Although each method has proven to work in some applications, they are most often focused on a point-based methodology. In large-scale applications, point-based sensors do not provide an accurate understanding of the spatial distribution of damage. This can be resolved if a large number of sensors are placed on the area of interest, however, that is rarely ideal in most civil and aerospace applications.

1.2 Fiber-Reinforced Polymer Composites

Over the past 50 years the usage of fiber-reinforced polymer composites has grown to an astounding value, and they are now seen in various applications including naval, aviation, civil, and transportation. In 2011, the Boeing 787 Dreamliner was released and contained 50 % composite material by weight as compared to the previous Boeing 777 which contained only 12 % composite material by weight [3]. This drastic increase in the use of composite materials in the aircraft industry has stirred a large debate on the understanding and safety of composite materials in a wide range of applications.

Composites are more appealing than traditional metals mostly due to their high strength-to-weight ratio. However, composites exhibit damage and failure modes such as delamination, dis-bonding, fiber pullout, matrix crazing, and micro-cracking, which are not observed in typical metals. As new failure modes are observed in composite materials, the integrity is somewhat challenged. Not only are these failure modes not easily detectable, but they are also not well understood. The common response of the public is very similar to that of Seattle Times aerospace reporter, Dominic Gates, where there is an unwavering doubt of how these composites may perform in a

crash, or even damage from a more common occurrence such as a bird collision during flight [25]. Another Seattle Times reporter, Mark Nowlin, has released computer generated drawings from a Boeing internal analysis showing that, during a crash landing, the passenger floor of a Boeing 777 may remain completely intact while that of the Boeing 787 will have collapsed [25]. Images such as these draw significant attention to the issues that we are facing with an increased use of composite materials in applications where even the slightest of damages can cause catastrophic failures.

1.3 Structural Health Monitoring

Structural health monitoring typically refers to an in-situ or continuous measurement of environmental and/or structural parameters during typical day-to-day operations. The purpose of SHM is to observe any abnormalities in a structure to prevent catastrophic failures. Through the use of SHM methods, early detection of minor and/or major failures in structures such as bridges, dams, aircraft, and pipelines can be observed prior to catastrophic failures in the systems. Currently, there are various types of SHM options for detecting and monitoring damage.

1.3.1 Strain gages

The use of strain gages in SHM applications stems from the demand of monitoring strain in a structure. Strain gages exhibit piezoresistive behavior where the resistance across the area varies linearly with the strain [8]. The most common strain gage is the bonded metallic strain gage which consists of a fine wire made of a metallic foil that is arranged in a serpentine pattern. The fine wire is bonded to a thin backing called a carrier, which allows for direct attachment to the sample or structure of interest. The bonded resistance strain gage is known to be very low in cost, of very small size and mass, and fairly sensitive to strain measurements [6]. In addition, by obtaining strain data measurements from a structure, the current stress state can be calculated based on certain assumptions.

Strain gages have been implemented for monitoring civil structures such as bridges, where they are applied to sections such as the rail track, bridge-deck trough, and rocker bearing links, among others [7]. The documentation of where the strain gages are located geometrically relative to the structure and other strain gages becomes fairly complex for determining damage location data. In addition, various data points are collected over the duration of days/weeks/months and an in-depth strain data reduction must be performed in order to isolate the useful data [7].

Overall, the use of strain gages is fairly limited due to their delicate nature, making them very easily ruined during manufacturing and application. In addition, their limited range creates the need for numerous strain gages on the surface of a structure in order to get an idea of its spatial strain distribution. This becomes less than ideal when looking at large, complex, geometry structures.

1.3.2 Optical Fiber-Based Sensors

Optical fiber-based sensors are currently used for monitoring structures such as The Alptransit project in Switzerland, the Plavinu dam on the Daugava River in Latvia, and the Horsetail Falls Bridge in the Colombia River Gorge National Scenic Area in the United States [10, 11]. Fiber optic sensors (FOSs) are popular due to their long life cycle, durability, resistance to corrosion, flexibility, and high tensile loading and temperature limits [10].

The basis of optical fiber-based sensing lies in their ability to detect the optical phase change induced in a light as it propagates along an optical fiber. The optical fiber is comprised of three layers: fiber core, cladding, and jacket. The fiber core and cladding are typically made of silica glass and must satisfy Snell's law where the refractive index of the fiber core is higher than the refractive index of the cladding to ensure propagation of light along the core only. The jacket is the outer layer and is usually made of a plastic that will provide mechanical strength to protect the optical fiber from being damaged. The different layers can be made of different materials that are determined by the application specifics. FOSs are sensitive enough to detect even the smallest perturbations due to changes in temperature, strains, electric and magnetic currents, and rotations in a structures. These perturbations can be analyzed as amplitude, phase, frequency, wavelength, and polarization changes in the optical properties from a transmitted light. These changes are analyzed by a demodulation system that can determine what the changes in such properties mean for the structural integrity of the system [10].

Applications are usually focused on the desired range of use and/or the type of data to be collected. There are a variety of FOSs in existence today, including the Fabry-Perot sensor, long gage sensor, fiber Bragg grating sensor, Raman/Rayleigh sensor, and the Brillouin sensor. The Fabry-Perot sensor is based on the white-light cross-correlation principle making it a great candidate in measuring strain, pressure, displacement, and temperature. The long-gage sensor is based on two low-coherent double Michelson interferometers that measure the average displacement observed between two fixed points that lie along the gage. The length of long-gage sensors are typically between 0.2 m to 50 m [11]. The fiber Bragg grating sensor is common in SHM applications today, since it can measure strains at multiple locations and is typically quasi-distributed. The fiber Bragg grating sensor produces

a wavelength change when light within the fiber interacts with an internal Bragg grating to cause a constructive interference between the forward wave of light and the contra-propagating wave of light. This interference leads to a narrowband reflection of light if the phase match condition is satisfied. Local strains and temperature changes can affect the grating period and thus the wavelength of the reflected light, allowing wavelength changes to occur and be analyzed by an interrogator or charged coupled device (CCD) spectrometer. In addition, various gratings with different paths can be arranged along an optical fiber to be able to detect various wavelength changes. Some errors are introduced into the system when using fiber Bragg grating sensors due to spectral overlap of the gratings and the interrogation filter. Fiber Bragg grating sensors are most commonly used to measure strain.

On the other hand, Raman/Rayleigh sensors are based on a transition or rotation in the vibrational levels of molecules induced by a temperature or strain change. The change in vibrational energy is analyzed using a high intensity optical pulse that induces a reflected Stokes and anti-Stokes signal that can be detected. The emitted light scattering from the optical pulse is typically on the scale of THz [13]. Raman/Rayleigh sensors can be used to measure both temperature and strain. The Brillouin sensor is based on Brillouin scattering, which results from an interaction between optical waves and sound waves within the optical fiber. Acoustic waves can be excited by changes in temperature/strain or by injecting two counter-propagating waves that have a frequency difference that is equal to the Brillouin shift. Issues with the Brillouin sensor stem from the low level (on the scale of MHz) of the detected signal requiring advanced signal processing techniques [11]. The type of sensor chosen is typically based on the measurands of interest, such as strain, displacement, and/or temperature [10].

In summary, FOSs have been implemented successfully into various applications. However, there are several disadvantages of FOSs that must be noted. The fragile nature of such fibers creates problems during manufacturing, packaging, and shipping [10]. FOSs are delicate in nature and can be damaged by exposure to water or alkalines from the host structure, often requiring additional sensor packaging to isolate the sensor. Also, it is important that the fiber, the sensor packaging, and the host structure all have similar thermal expansion coefficients to avoid issues of interfacial adhesion causing unreliable results [10]. The fragile nature of these FOSs makes them less than ideal in large scale applications where there is a risk for damage that could lead to limited sensing data. Lastly, authors such as Measures et al. [14] have noted that FOSs embedded in a structure can cause delamination in a lamina whereas authors such as Tsutsui et al. [15] have stated that using small-diameter FOSs on the order of 50 μm cause no negative effects on the mechanical properties of the lamina.

1.3.3 Electrical-Based Sensors

Electrical-based sensors are another form of SHM and can be derived from the inherent electrical properties of a structure or can stem from some conductive film being applied to a structure. The avenue of conductive thin films are gaining interest due to the benefits of applying the sensor to large-scale, complex, and both composite and metallic structures to monitor delamination, disbonding, and matrix micro-cracking, among others. Electrical-based sensors are based on the principle of correlating sensor electrical property changes to some external stimulus. To obtain an understanding of the strain state in a material, data collection is focused on the electrical resistance observed in the material. To collect the resistance in the material there are two well-known methods: two-probe method and four-probe method. The two-probe method contains connections at each end of the sample to measure voltage, although there are typically additional wires placed on the sample in order to pass current without taking into account the resistance of the wires in the measured resistance [26]. The four-probe method contains connections at each end which can either be attached as fiber end contacts or as perimeter contacts. In some rare cases, the four-probe contacts are placed perpendicular to the fiber direction so that resistance data can be collected through the thickness [27]. These wires serve to introduce a constant current into the system and measure the voltage output, which can be used to calculate the resistance using Ohm's Law. This method provides knowledge of the resistance within the structure and can monitor any changes that occur due to damages within the system.

A recent type of electrical-based sensor is centered on carbon fiber and carbon nanotube-based thin films due to their excellent electromechanical properties as well as their availability on the market today. Carbon fiber-reinforced polymer (CFRP) composites have been explored by Seo and Lee [27], where the inherent electrical resistance in the laminates was used to measure fatigue damage in the structure. Authors such as Thostenson and Chou [28] investigated the sensing capabilities of a glass fiber-epoxy composite that utilized multi-walled carbon nanotubes (MWCNT) distributed in the epoxy. By incorporating MWCNTs into the polymer matrix, a conductive network throughout the lamina was generated, which proved to be highly sensitive to matrix-dominated failure. It is also desirable to be able to monitor already existing structures using electrical-based sensing networks. For structures that are not inherently conductive, Loyola et al. [29, 30] were able to successfully produce a sprayable thin film from the addition of MWCNT into polyvinylidene fluoride (PVDF) solution. By producing a paint that is independently conductive, the paint can be sprayed onto non-conductive structures to allow for SHM of various systems.

1.3.4 Acoustic Emission and Ultrasonic-Based Sensor Networks

Acoustic emission (AE) and ultrasonic-based sensors are non-destructive testing methods to provide real-time data of the stress or strain state of the structure through the use of wave propagation. The sensor network chosen is based on the frequency of the waves that are propagated; acoustic waves have a frequency between 20 Hz and 20 kHz, whereas ultrasonic waves have a frequency between 20 kHz and 200 MHz. These sensing networks are different from the previously discussed sensing methods as the data is collected away from the actual location of the sensors. The transducers used are typically made of piezoelectric materials, which produce a voltage when a mechanical stress or strain is applied. Additionally, piezoelectric materials can be used as actuators where an applied voltage can induce a mechanical response [29]. Data is typically processed by using a waveform analysis to monitor any changes in the detected waves over some period of time.

AE and ultrasonic-based sensor networks can be implemented as passive or active systems. Passive systems incorporate various sensors that are distributed across a structure and wait for a stress wave to be induced from some type of damage within the structure. The signal can be captured by the sensors and used to identify the location and severity of the damage through advanced wave form analyses. For composite materials, some waves are characterized to signify things such as matrix cracking, delamination, disbonding, etc. Passive systems have a large disadvantage due to the need for an exact time synchronization among multiple sensors [19]. Active systems incorporate both sensors and actuators in order to detect damage. An active system can utilize the pitch-catch method where an actuator creates some strain in the structure and the various sensors instrumented on the structure measure how the wave interacts and propagates through the structure. An active system can also utilize the pulse-echo method, where one transducer can act as both the actuator to initiate a wave and also as a sensor to detect the wave.

Some of the targeted applications for AE and ultrasonic-based sensors are pipelines and wind turbine blades, as displayed by a system designed by Fraunhofer IZFP Dresden, which implements some of these techniques in combination with their current vibration analyses [22]. Marantidis et al. [20] investigated two AE techniques using narrowband transducers and wideband transducers for SHM of military aircraft. However, it is shown that an excessive number of sensors across the surface of the structure are often required to obtain useful data on the current state of stress and strain within the material [20-22]. In addition, the use of AE and ultrasonic based techniques have

been tried on complex geometries and anisotropic materials, however, due to the complex wave velocities and waveforms, it is very difficult to monitor such structures with these techniques [20].

1.3.4.1 Piezoelectric sensors in AE and Ultrasonics Applications

Piezoelectric materials are growing in popularity in sensing applications due to their capability of producing an electrical response when a mechanical strain is applied. Equally, piezoelectric materials can be used for actuation, where a time-varying electrical signal can be applied to produce a mechanical strain. Piezoelectric material-based sensors are used in SHM applications due to their lightweight, robust, and inexpensive nature [31]. Many piezoelectric sensors are currently used for detecting strain changes due to factors such as temperature, humidity, and strain resulting in a stress in a material which generates an electrical output. Most piezoelectric materials that are currently being researched or implemented into SHM systems are inorganic ceramics that have high electro-mechanical coupling factors. However, the industry is beginning to exploit piezoelectric characteristics observed in some polymers due to their greater flexibility and robustness.

Current piezoelectric sensors are produced from various types of ceramics including lead zirconate titanate (PZT) [9, 23, 32, 33], barium titanate ($BaTiO_3$) [34-36], zinc oxide (ZnO) [37, 38], and polymers such as PVDF [39-41]. Due to the brittle behavior of ceramic materials, the use of a piezoelectric polymer is much more appealing in most sensing and actuating applications. More specifically, the use of PVDF in piezoelectric sensing is of high interest due to the toughness, chemical inertness, and yield and useful operating strain [42]. By exploiting the piezoelectric capabilities of polymers like PVDF, the possibility of implementing a highly flexible piezoelectric sensor into large-scale complex geometry structures becomes more realistic.

1.4 Poly(vinylidene) Fluoride

1.4.1 Phase Types of PVDF

PVDF exists in four different phases, which are known as alpha, beta, gamma, and delta or phase II, I, III, and IV, respectively [43, 44]. The non-polar alpha phase of PVDF is the most commonly found form and can be obtained directly from the melt. Alpha phase is formed by $(CH_2\text{-}CF_2)_n$ chains in a $TGTG^{'}$ conformation and exhibits a monoclinic crystal lattice structure with lattice parameters a=4.96 Å, b=9.64 Å, and c=4.62 Å [44]. Alpha phase is the most common form due to its lower energy state and natural random orientation of the polymer chains [24, 45].

Beta phase is formed by an all trans chain in a TTT conformation in a zigzag planar structure resulting in an orthorhombic crystallographic form with lattice parameters a=8.58 Å, b=4.91 Å, and c=2.56 Å [44]. The last phase of interest for the purpose of this research is the gamma phase of PVDF. Gamma phase is formed by some combination of a TGTG' conformation with a T_3GT_3G' conformation and exhibits a monoclinic crystal structure with lattice parameters a=8.66 Å, b=4.93Å, and c= 2.58 Å [44]. The chemical structure of alpha and beta phase is shown in Figure 1.1. The conformation of gamma phase is best represented in 3-dimensional space as shown by Kobayashi et al. [44]. The conformation of some combination of beta and gamma phase is of importance in this study, as it lends to high values of electric polarization and therefore a dipole moment.

1.4.2 Characterization Methods of PVDF Phases

The phase of PVDF in a given specimen can be determined through various methods such as x-ray diffraction (XRD) [46-48], wide-angle x-ray diffraction (WAXD) [48], Fourier transform infrared spectroscopy (FTIR) [43, 44, 46], and Raman spectroscopy [24, 43, 46, 47]. The transition of alpha phase PVDF to some combination of beta and/or gamma phase PVDF occurs when the spherulites of the semi-crystalline sample are destroyed, thereby leading to a more fibrillar structure or aligned chain orientation. The detection of these phases using the various techniques described above is motivated by the molecular vibrations that occur due to the excitation of the method used [49]. The various types of characterization can be categorized into the field of vibrational spectroscopy, in which the study of the structure as well as the physiochemical properties of both crystals

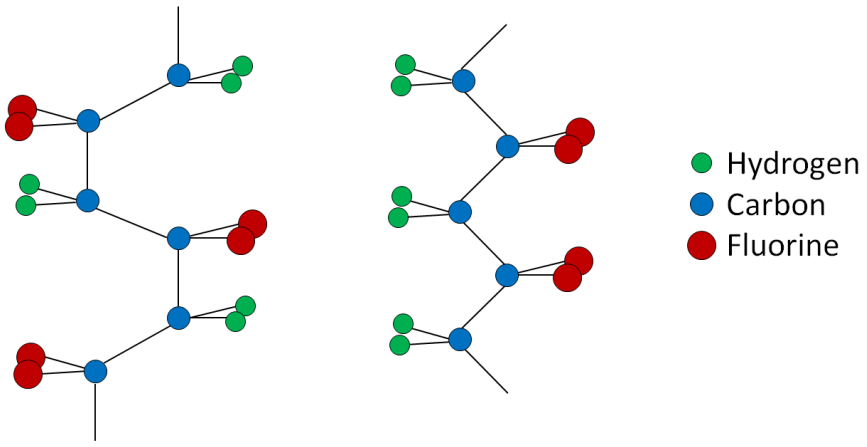

Figure 1.1: Chemical structure of non-polar alpha phase (left) and polar beta phase (right) PVDF

and molecular systems is examined [50].

1.4.2.1 X-ray Diffraction and Wide-Angle X-Ray Diffraction

The use of X-ray diffraction (XRD) and wide angle X-ray diffraction (WAXD) is common in characterizing the crystalline structure of various materials. An XRD instrument uses a diffractometer that has an X-ray beam of a single wavelength directed at the material. The x-ray beam incident angle is continuously changing during collection of a spectrum and the diffraction intensity for each angle is recorded. The final spectrum is a plot of incident angle versus diffraction intensity and is very useful in identifying the sample of interest since there are particular peaks associated with each material [51]. XRD is more commonly used with powder samples where WAXD is more commonly used with identifying the crystalline structure in both polymers and fibers. WAXD follows the same methodology of XRD, but the diffraction angle is $2\theta > 5^{\circ}$.

XRD methods can provide a significant amount of data about a material, including, the electron distribution in the atom, the arrangement of atoms within the crystalline structure, the bond angles, and the magnitude of thermal vibrations [52]. Depending upon the material of interest, the 2θ angle range can be chosen typically between 5°-65° so that the peaks characteristic of the material of interest are observed. The peaks observed from XRD and WAXD spectrum are directly characteristic of the stretching and bending of the molecules in the sample. For alpha phase PVDF there are diffraction peaks at 17.6°, 18.3°, 19.9° and 26.5°, which is different from that of beta phase where there are peaks observed at 20.57° and 36.3° [41]. XRD and WAXD peaks of beta phase and gamma phase are typically overlapping and not unique.

1.4.2.2 Raman Spectroscopy

The use of Raman spectroscopy for material characterization has been of growing importance in recent years due to the development and understanding achieved with new detectors and advanced lasers. Raman spectroscopy can be used in various applications for chemistry, biology, medicine, and materials science [53]. The convenience of Raman spectroscopy is the non-contact nature of the setup, thus allowing the user to characterize a variety of materials in solid, liquid, or gaseous states. For thin films, this is imperative as contact methods can deform thin films and bias the measurement.

Raman spectroscopy is the study of vibrational states within a material where electronic transitions can be measured from the activation of these vibrational states. The basic theory of Raman spectroscopy is best described by Jasinevicius [54], where the understanding of electromagnetic radiation has been linked to the understanding of vibrational activation. When the photons interact with atoms and molecules, there are two types of light scattering that can occur: Rayleigh scattering and Raman scattering. Rayleigh scattering is when the scattered photon retains the energy from the incident photon and there is no observed energy change; this is also known as elastic scattering. Raman scattering consists of both Stokes and anti-Stokes light scattering. Stokes scattering refers to the scattering in which atoms in the specimen absorb energy from light, and the atoms are elevated to a higher energy vibrational state. The reflected light loses energy relative to its original state and is shifted toward the greater light wavelengths end of the electromagnetic spectrum. Anti-Stokes scattering refers to the scattering that occurs when energy is transferred from atoms that are already excited to the incident photon, so that atoms associated with a specific vibration are pushed to a lower energy vibrational state. The reflected light is higher in energy than the Rayleigh line, so the wavelength is shifted toward the blue end of the electromagnetic spectrum. This is not as common as Stokes scattering, as it requires that the atoms be in a higher energy state prior to laser activation.

Since not all materials have the same vibrational capabilities, not all materials are considered to be "Raman active." For a material to be Raman active, the atoms must begin to oscillate when the incident beam interacts with the atoms. As the atom oscillates, the electrons are forced to move in different directions to cause a change in the electron cloud. This movement creates a separation of charge in the atom, resulting in a dipole (*i.e.*, the atom becomes polarized). This change in polarization of the bonded atoms causes a material to be Raman active.

In Raman spectra there are particular bands characteristic of different stretching, rocking, and vibrating modes. In particular, there is a very intense and sharp peak observed at 794 cm^{-1} that is associated with a CH_2 rocking vibration characteristic of alpha phase PVDF. In addition, there is a medium Raman peak observed at 839 cm^{-1} that is due to a mixture of CF_2 stretching, CC stretching, and CH_2 rocking characteristic of beta phase PVDF [24, 50]. These distinguishable peaks are shown in Figure 1.2 where the characteristic alpha peak is observed at 794 cm^{-1}, and the characteristic beta peak is observed at 839 $cm^{-}1$. As in XRD and WAXD, the beta phase and gamma phase peaks typically overlap and are not unique in Raman spectroscopy.

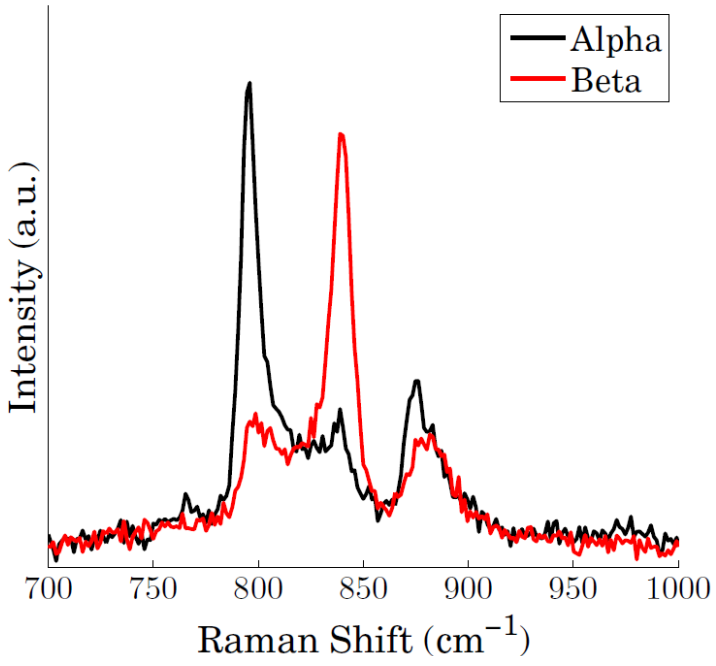

Figure 1.2: Characteristic Raman spectra of alpha and beta phase PVDF

1.4.2.3 Fourier Transform Infrared Spectroscopy

Fourier transform infrared spectroscopy discovery dates back to the 19th century with a basis in an understanding of the Michelson interferometer invented by Albert Abraham Michelson [55]. The Michelson interferometer was not initially designed to perform infrared spectroscopy. Initially, the interferograms were manually measured and could be converted, very tediously, into a spectrum. It was not until computers became more common that the spectra became more popular due to the faster computing speeds of the Fourier transforms [55]. Since the 19th century, there have been major advances in FTIR that make the collection of spectra so easy today.

FTIR specifically measures the frequency dependence of the interaction of radiation with the matter or sample of interest [56]. Most FTIR instruments contain a Michelson interferometer that emits an infrared light source onto a cylindrical beam. The light source is split by a beam-splitter and projected onto a fixed mirror and a moving mirror. The reflectance of the split infrared light produces an interference pattern to be analyzed. The reflected light has a unique pattern since each sample will absorb infrared light at a different intensity for each particular frequency. Once the sample reflects and/or absorbs certain frequencies of the light, the interferogram signal is transform into an electrical signal. The electrical signal data is then fast Fourier transformed with the Cooley-Turkey algorithm leaving the spectra that is commonly used today [56].

Scientists have defined that there are three different regions when analyzing an FTIR spectra. The infrared region is from 12800 to 10 cm^{-1} overall, which can be divided into the near-infrared region (12800 to 4000 cm^{-1}), the mid-infrared region (4000 to 200 cm^{-1}), and the far-infrared region (1000 to 50 cm^{-1}), with the most commonly used region lying between 4000 and 400 cm^{-1} [57]. Infrared spectrum is known as a vibrational spectrum much like Raman spectroscopy. Infrared light can be absorbed by a molecule causing the molecules to transfer from a ground state to an excited state. The excited state of the molecule leads to a vibrational energy gap causing a unique absorption peak at a particular frequency. The use of FTIR is important in distinguishing the existence of beta and/or gamma. This sensitivity is different than that of Raman spectroscopy due to the prominent band observed at 1234 cm^{-1} for gamma, as compared to the band observed at 1275 cm^{-1} for beta [58] (Figure 1.3). The remaining characteristic band peaks of both beta and gamma tend to overlap, which causes some difficulty in identifying which phase is predominant in the material [58]. This extra peak is unique to either beta and/or gamma providing some reassurance of which dominates the PVDF sample of interest.

1.4.3 Methods to Induce PVDF Phase Change

The purpose of inducing a phase change in a PVDF thin film or PVDF-based material is typically due to the need for the material to exhibit a more crystalline structure to be able to exhibit polarizable or piezoelectric

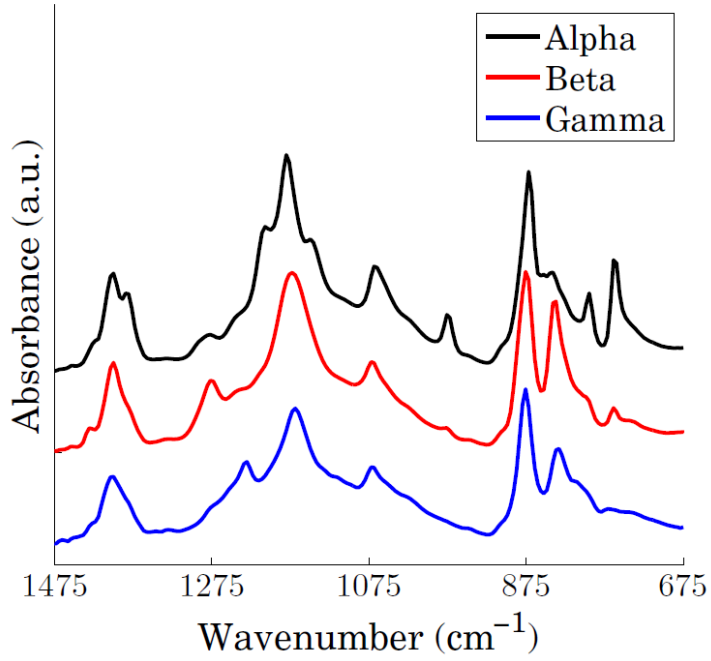

Figure 1.3: Characteristic FTIR scans of three phases of PVDF

characteristics. Since PVDF can exist in four different phases (*i.e.* alpha, beta, gamma, and delta), there are various methods to induce a phase change. Most methods stem from two basic ideologies, namely, mechanical stretching and chemical composition.

1.4.3.1 Mechanical Stretching

The most common transition from alpha phase to beta phase PVDF is achieved through mechanical stretching. Mechanical stretching is typically achieved by placing a sample under tensile loading with or without heat [41, 43, 47, 49]. During the 1980's, Matsushige et al. [47] worked on the alpha to beta phase transition using both tensile and compressive stresses in a range of temperatures. The work concluded that the sample deformed during cold drawing, and the beta phase was detected where necking was initiated in the sample (to be discussed more thoroughly in Chapter 2). In addition, Matsushige et al. [47] confirmed that beta phase PVDF films could also be formed by applying compression forces to the sample. Also, if the sample was exposed to a high direct current (DC) voltage, a highly uniaxially oriented film of beta phase would be formed that would display superior piezoelectric properties [47]. An *in situ* study was performed by Riosbaas et al. [49] that provided Raman spectra to characterize the alpha to beta phase transition during tensile loading. The work reported that only a stretch ratio of 1.5 was necessary for phase transition, and that beta phase was only detected in the necking region of the thin film [49]. Lastly, Salimi and Yousefi [43] performed a focused study on the relationship between stretching and heating and provided a conclusion that an increase in temperature required an increase in stretch ratio (*i.e.* greater than 5) for the transition from alpha phase to beta phase.

Another form of mechanical deformation was introduced by Nasir et al. [59] using electrospray deposition (ESD) where the mechanical deformation was introduced as the solution experiences electrostatic forces creating surface tension. The ESD process provided an interesting alternative to mechanical deformation of the polymer, where the polymer was placed in a nozzle and exposed to a strong electric field. The electrostatic forces produced within the polymer caused a high surface tension on the solution. The high surface tension caused charged droplets to spray from the nozzle and to collect on a conductive substrate forming a thin film of PVDF that was confirmed as beta phase by using WAXD [59].

A slightly varied approach to the electrospray method used by Nasir et al. [59] is shown by Costa et al. [60] where the polymer solution of PVDF was added to a syringe with a needle and then placed under a high voltage ranging from 5 to 30 kV while being exposed to high temperatures for solvent evaporation. The electric charges

were forced to accumulate in the droplet at the end of the syringe, which caused an electrostatic repulsion in the droplet and forced it into a cone shape. The solution used was sufficiently viscous so that the polymer would severely stretch before extruding as a jet stream out of the needle. This caused the formation of beta phase PVDF to be produced. However, the conclusions of the work by Costa et al. [60] directly contradict that of Nasir et al. [59], where Costa et al. [60] claims that the solvent evaporation rate and not the extrusion (and thus, mechanical deformation) was the cause of the beta phase formation. In addition, some effect of solvent evaporation was also observed by Sundaray et al. [61] while electrospinning PVDF cast from DMF solutions.

A slightly different approach was taken by Haghiashtiani et al. [39] where a composite layup was created and then cured under high temperatures and high pressures to produce beta phase PVDF. On the top and bottom of the PVDF layers, a carbon fiber layer was placed in order to act as a top and bottom electrode for the sample to be polarized. This approach created an embedded PVDF layer within the composite layup that displayed piezoelectric properties. The key to this approach must be emphasized as the application of high pressure during curing generating a mechanical stretching phenomenon [39].

1.4.3.2 Chemical Composition

The most common method to induce a phase change in PVDF is to use the copolymer of polyvinylidene fluoride-trifluoroethylene (PVDF-TrFE), which has a higher tendency of beta phase formation. Dodds et al. [62] was able to do this by spin coating dispersed zinc oxide (ZnO) nanoparticles in a PVDF-TrFE based solution that would enhance the piezoelectric properties due to the beta phase content as well as the piezoelectric capabilities of ZnO nanoparticles. Meyers et al. [38] expanded on this application by poling these thin films and applying them in active sensing and damage detection applications such as a pitch-catch setup on an aluminum plate and pipe. The ZnO/PVDF-TrFE thin films produced were proven to be capable of use as piezoelectric transducers.

The addition of organically modified silicates (OMS) is very popular in a research group led by Peggy Cebe from Tufts University, where the addition of very small concentrations of OMS were reported to aid in the formation of beta phase PVDF [58, 63-65]. Concentrations of 0.01 to 20 % by weight of OMS were added to PVDF that was suspended in a dimethyl acetamide (DMAc) solvent. Upon baking out the solvent, beta phase PVDF was resulting in thin films cast into petri dishes. Buckley et al. [63] concluded that at concentrations below 0.025 % by weight, alpha phase dominated, where anything higher led to a dominating beta phase. These films were confirmed using WAXS and FTIR.

In addition, investigations have been performed on the effect of adding MWCNTs to PVDF blends in order to optimize the crystallization. Kim et al. [66] was able to do this successfully and found that when MWCNTs were added up to 0.2 % by weight, they acted as a nucleating agent resulting in a higher beta phase formation in poled and drawn samples. However, if greater concentrations of MWCNTs were added, depolarization was induced as was the beta phase content. In the paper by Kim et al. [66], it was stated that even in samples with optimal MWCNT concentrations, little beta phase existed prior to mechanically stretching the sample. Huang et al. [67] was able to confirm this conclusion, where there is negligible effect of beta phase formation in the PVDF samples prior to mechanically stretching the sample. However, Huang et al. [67] was able to conclude that the dynamic storage modulus and thermal stability were both improved with the addition of MWCNTs.

In a paper by Gregorio and Nociti [68], the effect of adding various concentrations of poly(methyl methacrylate) (PMMA) were studied. It was reported that if concentrations lower than 30 % by weight of PMMA were added to PVDF, the beta phase could be produced directly from the melt. This blend was desirable as the thin film that was produced was partially crystalline. Further, it was shown that different concentrations of PMMA cured at different temperatures could produce different concentrations of alpha/beta phase, which were confirmed by thermograms and XRD spectrum.

1.4.4 Methods to Pole PVDF

In order for PVDF to behave as a piezoelectric material, the chain must first be aligned to a crystalline structure by activating a phase change transition from alpha phase to beta phase. Following the phase change transition, it is necessary to pole the material to align the dipoles so that it can exhibit piezoelectric behavior. There are two common methods that are used to pole PVDF.

1.4.4.1 Dielectric Poling

Dielectric poling is performed using a top and a bottom electrode on either side of the piezoelectric layer in order to align the dipoles in an oriented manner. Authors such as Egusa and Iwasawa [69] performed this task by applying a PZT/epoxy piezoelectric paint to an aluminum beam to serve as the bottom electrode and applying silver ink on top of the film to form the top electrode. Their poling setup was performed at room temperature with a high voltage power supply set for 240 kV/cm for 5 min [69]. Payo and Hale [9] used a similar setup with dielectric poling of a PZT ceramic powder suspended in a water-based acrylic polymer. Their piezoelectric paint was cured on an

aluminum substrate to serve as the bottom electrode and was topped with a matrix of water-based acrylic polymer with metallic pigments homogenously distributed. Payo and Hale [9] used a high voltage power supply where voltages of 9 kV/mm were applied at room temperature.

It is important to note that the voltages reported were typically based on the thickness and formulation of their respective paint. However, the use of an aluminum substrate and a small metallic conducting electrode as the bottom and top electrodes was very common in dielectric poling for various piezoelectric materials [23, 70, 71].

1.4.4.2 Corona Poling

Corona poling is slightly different than dielectric poling as it is a non-contact method of poling piezoelectric materials. According to Mahadeva et al. [72], dielectric poling often leads to electric breakdown, since such large voltages were required for poling piezoelectric materials. Dielectric breakdown occurs when a conductive path is formed through the thickness of the film, and electrons were allowed to flow freely between the two surfaces of the conductive electrodes from a minimal applied voltage. Mahadeva et al. [72] stated that, although corona poling involves a strong electric field, there were fewer charge carriers than with dielectric poling and electric breakdown issues were reduced. Similarly, authors such as Costa et al. [73] confirmed the benefit of Corona poling and stated that the tendency to produce dielectric failure was much lower since there was a low mobility of charges on the non-metallized surface.

The basis of Corona poling relies on the ability to ionize air molecules above a material. The air molecules are ionized by applying a large DC voltage to a set of needles that causes an ionization of the gas molecules surrounding the needles. This typically takes place in a poling apparatus to isolate the Corona poling to a particular area [74]. Mohammadi et al. [41] were able to successfully pole a beta phase PVDF thin film using Corona poling by applying an electric field of 1.8 MV/cm for 10 minutes at a 103 ˚C to an already stretched sample. From this exposure, they were able to obtain the stress piezoelectric coefficients confirming piezoelectricity in the stretched thin films. Authors such as Kenney et al. [75] stated that higher temperatures were not necessary depending upon the Corona poling setup that wass used and the time exposure implemented.

1.5 Key Contributions of this Thesis and Conclusions

In this work, we want to leverage the previous work in piezoelectric-based impact detection sensors to develop a spray-deposited sensor that can be easily deposited over large areas for *in situ*, spatially distributed, impact detection. Polyvinylidene fluoride thin films are promising for this application due to their ability to demonstrate piezoelectric properties, as well as their flexibility, resistance to creep, and toughness [46].

In order for PVDF thin films to possess piezoelectric properties, it is necessary for the PVDF thin film to undergo a phase change from the most commonly found alpha phase to some combination of the polarizable beta and/or gamma phase [24, 45]. This has been done primarily by mechanical stretching of the film where the initial and final phase is characterized by means of Fourier transform infrared spectroscopy, X-ray diffraction, wide-angle X-ray diffraction, and Raman spectroscopy [24, 43, 47]. This work focuses on the various methods of phase change and characterization in PVDF thin films. With the desirability of a sprayable sensing film in mind for large-scale, complex geometry structures, an initial focus of mechanically stretching pure PVDF thin films and using Raman spectroscopy for characterization was done as a base reference. Since the application onto large structures would prohibit mechanical stretching post-application, this work led to the focus of a sprayable PVDF-based thin film that would undergo a phase change by other means and was characterized using Fourier transform infrared spectroscopy.

To explore methods of phase change activation in PVDF thin films without incorporating mechanical stretching, an experimental setup that simultaneously applied high voltage in a high temperature environment was implemented. Upon testing various combinations of voltages and temperatures no phase change was observed. To maintain the goal of a sprayable sensor, chemical composition became a priority as the phase change activation could potentially be achieved with some chemicals. This avenue, again, resulted in no successful phase change. Through the various trials conducted for the purpose of this thesis, we are able to come to a confident conclusion that the phase change activation in PVDF thin films stems from mechanical deformation only, despite publications from various research groups.

Chapter 1 References:

1. Engineers, A.S.o.C. *Report Card for America's Infrastructure*. 2013 06/17/2014].
2. Shalal-Esa, A., *Exclusive: U.S. sees lifetime cost of F-35 fighter at $1.45 trillion* Reuters, 2012.
3. Hale, J., *Boeing 787 From the Ground Up.* AeroMagazine A Quarterly Publication, 2006(QTR_04): p. 15-23.
4. Gates, D. *Composite material used in Boeing 787 raises safety questions Unique carbon-fiber makeup of Boeing 787's raises safety concerns*. Chicago Tribune-Business, 2010.
5. Hu, N., et al., *An efficient approach for identifying force using embedded piezoelectric sensors.* International Journal of Impact Engineering, 2007. **34**: p. 1258-1271.
6. *Strain Gage Technical Data - Strain Gage Measurement*. 2014 [cited 2014 06/24/2014]; Available from: http://www.omega.com/techref/strain-gage.html.
7. Chan, T.H.T., Z.X. Li, and J.M. Ko, *Fatigue analysis and life prediction of bridges with structural health monitoring data- Part II: application.* International Journal of Fatigue, 2001. **23**: p. 55-64.
8. *Strain Gauge Measurement- A Tutorial*. 1998, National Instruments. p. 1-12.
9. Payo, I. and J.M. Hale, *Sensitivity analysis of piezoelectric paint sensors made up of PZT ceramic powder and water-based acrylic polymer.* Sensors and Actuators A: Physical, 2011. **168**: p. 77-89.
10. Li, H.-N., D.-S. Li, and G.-B. Song, *Recent applications of fiber optic sensors to health monitoring in civil engineering.* Engineering Structures, 2004. **26**: p. 1647-1657.
11. Inaudi, D. and B. Glisic. *Overview of Fibre Optic Sensing Applications to Structural Health Monitoring*. in *Measuring the Changes 13th Symposium on Deformation Measurement and Analysis*. 2008. LNEC, Lisbon.
12. Sidek, O., S. Kabir, and M.H.B. Afzal. *Fiber Optic-based Sensing Approach for Corrosion Detection*. in *PIERS* 2011. Suzhou, China.
13. Bao, X. and L. Chen, *Recent Prgress in Distributed Fiber Optic Sensors.* Sensors 2012. **12**: p. 8601-8639.
14. Measures, R., et al., *Structurally integrated fiber optic damage assessment system for composite materials.* Applied Optics, 1989. **28**(13): p. 2626-2633.
15. Tsutsui, H., et al. *Real-Time Detection of Impact Load on composite Laminates with Embedded Small-Diameter Optical Fiber*. in *Smart Structures and Materials 2000*. 2000.
16. Li, X. and Y. Zhang, *Piezoelectric paint sensor for ultrasonic NDE.* Sensors and Smart Structures Technologies for Civil, Mechanical, and Aerospace Systems, Proc. of SPIE, 2007. **6529-04**: p. 1-11.
17. Yoo, B., et al., *Piezoelectric-paint-based two-dimensional phased sensor arrays for structural health monitoring of thin panels.* Smart Materials and Structures, 2010. **19**: p. 1-15.
18. Zhang, Y., *In Situ Fatigue Crack Detection using Piezoelectric Paint Sensor.* Journal of Intelligent Material Systems and Structures, 2006. **17**: p. 843-851.
19. Grosse, C.U., S.D. Glaser, and M. Kruger, *Initial development of wireless acoustic emission sensor Motes for civil infrastructure state monitoring.* Smart Structures and Systems, 2010. **6**(3): p. 197-209.
20. Marantidis, C., C.B.V. Way, and J.N. Kudva. *Acoustic-emission sensing in an on-board smart structural health monitoring system for military aircraft*. in *Smart Structures and Materials: Smart Sensing, Processing, and Instrumentation*. 1994.
21. Prevorovsky, Z., et al. *Structural Health Monitoring in aerospace and civil engineering supported with two ultrasonic NDT methods - AE and NEWS*. in *International Workshop of NDT Experts, 6th NDT in Progress*. 2011. Prague, Czech Republic.
22. Meyendorf, N., B. Frankenstein, and L. Schubert. *Structural Health Monitoring for Aircraft, Ground Transportation Vehicles, Wind Turbines and Pipes - Prognosis*. in *18th World Conference on Nondestructive Testing*. 2012. Durban, South Africa.
23. Payo, I. and J.M. Hale, *Dynamic characterization of piezoelectric paint sensors under biaxial strain.* Sensors and Actuators A: Physical, 2010. **163**: p. 150-158.
24. Constantino, C.J.L., et al., *Phase Transition in Poly(vinylidene fluoride) Investigate with Micro-Raman Spectroscopy.* Applied Spectroscopy, 2005. **59**(3): p. 275-279.

25. Gates, D. *How will 787's new material fare in a crash landing*. The Seattle Times- Business/Technology, 2010.
26. Wang, S. and D.D.L. Chung, *Piezoresistivity in Continuous Carbon Fiber Polymer-Matrix Composite.* Polymer Composites, 2000. **21**(1): p. 13-19.
27. Seo, D.-C. and J.-J. Lee, *Damage detection of CFRP laminates using electrical resistance measurement and neural network.* Composite Structures, 1999. **47**: p. 525-530.
28. Thostenson, E.T. and T.-W. Chou, *Carbon Nanotube Networks: Sensing of Distributed Strain and Damage for Life Prediction and Self Healing.* Advanced Materials, 2006. **18**: p. 2837-2841.
29. Loyola, B.R., *Distributed In Situ Health Monitoring of Conductive Self-Sensing Fiber-Reinforced Polymers Using Electrical Impedance Tomography*, in *Mechanical and Aeronautical Engineering*. 2010, University of California at Davis: Davis, CA. p. 92.
30. Loyola, B.R., et al., *The electrical response of carbon nanotube-based thin film sensors subjected to mechanical and environmental effects.* Smart Materials and Structures, 2013. **22**.
31. Park, G., et al., *Overview of Piezoelectric Impedance-Based Health Monitoring and Path Forward*, in *The Shock and Vibration Digest*. 2003. p. 451-463.
32. White, J.R., et al., *Piezoelectric paint: Ceramic-polymer composites for vibration sensors.* Journal of Materials Science, 2004. **39**: p. 3105-3114.
33. Lahtinen, R., et al., *A piezopaint-based sensor for monitoring structure dynamics.* Smart Materials and Structures, 2007. **16**: p. 2571-2576.
34. Capurso, J.S., A.B. Alles, and W.A. Schulze, *Processing of Laminated Barium Titanate Structures for Stress-Sensing Applications.* Journal American Ceramics Society, 1995. **78**(9): p. 2476-2480.
35. Karaki, T., K. Yan, and M. Adachi, *Barium Titanate Piezoelectric Ceramics Manufactrued by Two-Step Sintering.* Japanese Journal of Applied Physics, 2007. **46**(1): p. 7035.
36. Ertug, B., *The Overview of The Electrical Properties of Barium Titanate.* American Jounral of Engineering Research 2013. **2**(8): p. 1-7.
37. Loh, K.J. and D. Chang, *Zinc oxide nanoparticle-polymeric thin films for dynamic strain sensing.* Journal of Materials Science, 2011: p. 228-237.
38. Meyers, F.N., et al., *Active sensing and damage detection using piezoelectric zinc oxide-based nanocomposites.* Nanotechnology, 2013. **24**: p. 1-10.
39. Haghiashtiani, G., M.A. Greminger, and P. Zhao, *Poling of PVDF matrix composites for integrated structural load sensing.* Sensors and Smart Structures Technologies for Civil, Mechanical, and Aerospace Systems, Proc. of SPIE, 2014. **9061-27**: p. 21-29.
40. Jain, A., et al., *Detailed studies on the formation of piezoelectric beta-phase of PVDF at different hot-stretching conditions.* Sensors and Smart Structures Technologies for Civil, Mechanical, and Aerospace Systems, Proc. of SPIE, 2010. **7647-2C**: p. 1-11.
41. Mohammadi, B., A.A. Yousefi, and S.M. Bellah, *Effect of tensile strain rate and elongation on crystalline structure and piezoelectric properties of PVDF thin films.* Polymer Science Direct, 2007. **26**: p. 42-50.
42. Thompson, M.L., *On the Material Properties and Constitutive Equations of Piezoelectric Poly Vinylidene Fluoride (PVDF)*, in *Mechanical Engineering*. 2002, Drexel University: Philadelphia, Pennsylvania. p. 176.
43. Salimi, A. and A.A. Yousefi, *FTIR Studies of beta-phase crystal formation in stretched PVDF films.* Polymer Science Direct, 2003. **22**: p. 699-704.
44. Kobayashi, M., K. Tashiro, and H. Tadokoro, *Molecular Vibrations of Three Crystal Forms of Poly(vinylidene fluoride)* Macromolecules, 1974. **8**(2): p. 158-171.
45. Constantino, C.J.L., et al., *The Investigation of alpha to beta Phase Transition in Poly(Vinylidene) Fluoride (PVDF).* Electrets ISE-12 12th International Symposium, 2005: p. 178-181.
46. Jain, A., et al., *Detailed studies on the formation of piezoelectric beta-phase of PVDF at different hot-stretching conditions.* Sensors and Smart Structures Technologies for Civil, Mechanical, and Aerospace Systems, Proc. of SPIE, 2010. **7647**: p. 2C-1-2C-11.
47. Matsushige, K., et al., *The II-I crystal transformation of poly(vinylidene fluoride) under tensile and compressional stresses.* Polymer Journal, 1979. **21**: p. 1391-1397.
48. Vijayakumar, R.P., D.V. Khakhar, and A. Misra, *Studies on alpha to beta Phase Transformations in Mechanically Deformed PVDF Films.* Journal of Applied Polymer Science, 2010. **117**: p. 3491-3497.
49. Riosbaas, M.T., et al. *In situ phase change characterization of PVDF thin films using Raman spectroscopy*. in *Sensors and Smart Structures Technologies for Civil, Mechanical, and Aerospace Systems*. 2014.

50. Nallasamy, P. and S. Mohan, *Vibrational spectroscopic characterization of form II poly(vinylidene fluoride).* Indian Journal of Pure & Applied Physics, 2005. **43**: p. 821-827.
51. Leng, Y., *Materials Characterization Introduction to Microscopic and Spectroscopic Methods*. Second ed. 2013, Weinheim, Germany: Wiley-VCH. 367.
52. Warren, B.E., *XRay Diffraction Methods.* Journal of Applied Physics, 1941. **12**: p. 375-384.
53. Ferraro, J.R., K. Nakamoto, and C.W. Brown, *Introductory Raman Spectroscopy*. 2003, Massachusetts: Academic Press.
54. Jasinevicius, R., *Characterization of Vibrational and Electronic Features in the Raman Spectra of Gem Minerals*, in *Department of Geosciences*. 2009, The University of Arizona. p. 147.
55. Smith, B.C., *Fundamentals of Fourier Transformed Infrared Spectroscopy*. 1996: CRC Press LLC.
56. Leclerc, D.F., *Fourier Transformed Infrared Spectroscopy in the Pulp and Paper Industry*, in *Encyclopedia of Analytical Chemistry*, R.A. Meyers, Editor. 2000, John Wiley & Sons Ltd: Chichester. p. 8361-8388.
57. Shaikh, T.A. and S.A. Agrawal, *Qualitative and Quantitative Characterization of Textile Material by Fourier Transformed Infra-Red.* International Journal of Innovative Research in Science, Engineering and Technology, 2014. **3**(1): p. 8496-8502.
58. Ince-Gunduz, B.S., et al., *Impact of Nanosilicates on poly(vinylidene fluoride) crystal polymorphism: Part 1. Melt-crystallization at high supercooling.* Polymer Science Direct, 2010. **51**: p. 1485-1493.
59. Nasir, M., et al., *Control of Diameter, Morphology, and Structure of PVDF Nanofiber Fabricated by Electrospray Deposition.* Journal of Polymer Science: Part B: Polymer Physics, 2006. **44**: p. 779-786.
60. Costa, L.M.M., R.E.S. Bretas, and R.G. Jr., *Effect of Solution Concentration on the Electrospray/Electrospinning Transition and on the Crystalline Phase of PVDF* Materials Sciences and Applications, 2010. **1**: p. 247-252.
61. Sundaray, B., et al., *Unusual process-induced curl and shrinkage of electrospun PVDF membranes.* Polymer Journal, 2013. **54**: p. 4588-4593.
62. Dodds, J.S., F.N. Meyers, and K.J. Loh, *Piezoelectric nanocomposite sensors assembled using zinc oxide nanoparticles and poly(vinylidene fluoride).* Smart Structures and Systems, 2013. **12**(1): p. 1-17.
63. Buckley, J., et al., *Nanocomposites of poly(vinylidene fluoride) with organically modified silicate.* Polymer Science Direct, 2006. **47**: p. 2411-2422.
64. Cebe, P. and J. Runt, *P(VDF-TrFE)-layered silicate nanocomposites. Part 1. X-ray scattering and thermal analysis studies.* Polymer Science Direct, 2004. **45**: p. 1923-1932.
65. Ince-Gunduz, B.S., et al., *Impact of Nanosilicates on Poly(vinylidene fluoride) Crystal Polymorphism: Part 2. Melt-crystallization at Low Supercooling.* Journal of Macromolecular Science, Part A: Pure and Applied Chemistry, 2010. **47**: p. 1208-1219.
66. Kim, G.H., S.M. Hong, and Y. Seo, *Piezoelectric properties of poly(vinylidene fluoride) and carbon nanotube blends: beta-phase development.* Physical Chemistry Chemical Physics, 2009. **11**: p. 10506-10512.
67. Huang, W., et al., *Nanocomposites of Poly(vinylidene fluoride) with Multiwalled Carbon Nanotubes.* Journal of Applied Polymer Science, 2009. **115**: p. 3238-3248.
68. Jr., R.G. and N.C.P.d.S. Nociti, *Effect of PMMA Addition on the solution crystallization of the alpha and beta phases of poly(vinylidene fluoride) (PVDF).* Journal of Applied Physics, 1995. **28**: p. 432-436.
69. Egusa, S. and N. Iwasawa, *Poling Characteristics of PZT/Epoxy Piezoelectric Paints.* Ferroelectrics, 1993. **145**: p. 45-60.
70. Sencadas, V., et al. *Poling of beta-poly(vinylidene fluoride): dielectric and IR spectroscopy studies*. in *12th Annual POLYCHAR World Forum on Advanced Materials*. 2004. Guimaraes, Portugal.
71. Ploss, B., et al., *Poling study of PZT/P(VDF-TrFE) composites.* Composites Science and Technology, 2001. **61**: p. 957-962.
72. Mahadeva, S.K., et al., *Effect of poling time and grid voltage on phase transition and piezoelectricity of poly(vinylidene fluoride) thin films using corona poling.* Journal of Physics D: Applied Physics, 2013. **46**: p. 1-7
73. Costa, M.M. and J.A. Giacometti, *Electric-field-induced phase changes in polyvinylidene fluoride: Effects from corona polarity and moisture.* Applied Physics Letters, 1993. **62**(10): p. 1091-1093.
74. Hanner, K.A., et al., *Thin film 0-3 Polymer/Piezoelectric Ceramic Composites: Piezoelectric Paints.* Ferroelectrics, 1989. **100**: p. 255-260.
75. Kenney, J.M. and S.C. Roth, *Room Temperature Poling of Poly(Vinylidene Fluoride) with Deposited Metal Electrodes.* Journal of Research of the National Bureau of Standards, 1979. **84**(6): p. 447-453.

Chapter 2: In Situ Phase Change Characterization of PVDF Thin Films Using Raman Spectroscopy

This chapter is based on a paper that has been submitted and published in the conference proceedings of the SPIE Smart Materials and Structures Conference. In the paper, I am first author, and I have carried out the experimental work and analysis of the results[1].

2.1 Introduction

The development of a piezoelectric impact detection sensor is desired for aerospace, civil, and military applications, among others. Implementation of a PVDF based architectural coating is ideal for such a purpose as it is designed to be easily deposited on complex geometries, be mechanically robust, and piezoelectric properties can be induced into the coating. In order to utilize PVDF as a sensor, the polymer must be converted from typical alpha phase to beta phase prior to electrostatic poling. This research focuses on the in situ characterization of mechanical activation of the beta phase in a non-sprayable PVDF thin film using *in situ* Raman spectroscopy for real-time monitoring of PVDF phase content. The PVDF thin films were experimentally characterized as freestanding thin films drawn in a tensile stage, while *in situ* Raman spectroscopic measurements were obtained at a wavelength of 532 nm. The Raman spectrum of each phase of PVDF is known to be unique and was correlated with the amount of alpha and beta phases in the characterized film during and after phase transition. The load and strain data from the tensile stage was associated with the *in situ* Raman spectra of the PVDF, thereby providing a relationship between load, strain, and beta phase content in these PVDF thin films.

[1] The information presented herein has been previously published by the following: Riosbaas, M.T., Loh, K.J., O'Bryan, G., Loyola, B.R., *In situ phase change characterization of PVDF thin films using Raman spectroscopy.* Sensors and Smart Structures Technologies for Civil, Mechanical, and Aerospace Systems, Proc. of SPIE, 2014. **9061**.

2.2 Experimental Details

2.2.1 PVDF Thin Film

A commercially available PVDF thin film of alpha phase was purchased from McMaster-Carr for this study. The material properties are provided in table 1. Sheet PVDF was studied as a precursor to spray-deposited PVDF-based thin films due to their progressive phase transition when evaluated using *in situ* monitoring without the complexity of the chemical makeup of sprayed thin films. This PVDF thin film is made from Solef resin grade 9009 and is 0.254 mm thick. The samples were cut into dog bone shapes using a dog bone punch from ASTM D-1708.

2.2.2 Micro-Tensile Load Testing

A 100 lb tensile stage micro-load frame from MTI instruments was used for the entirety of this study. The nominal strain travel of this load frame is 27.178 mm, and the dog bone samples were extended to maximum strain on the load frame. A strain rate of 50.8 mm•min^{-1} was utilized, as strain rate dependence does not play a role in this study [1].

The micro-load frame was commanded to pause at specific time intervals in order to obtain *in situ* Raman spectra measurements. The sample was elongated in 25.4 mm intervals and then paused for the Raman scan to take place. The pauses were implemented to hold the sample statically during the Raman measurements, which took 15 s.

Table 2.1: Properties of Solef 1010 Pure PVDF Homopolymer made from Solef Resin Grade 9009

Physical Properties		
Yield	565 m^2/kg/μm	internal
Melting Point	170-174 ˚C	ASTM D3418
Mechanical Properties at 23℃		
Stress at Yield	55-56 MPa	ASTM D882
Elongation at Yield	6-6.2%	ASTM D882
Stress at Break	54-57 MPa	ASTM D882
Elongation at Break	200-250%	ASTM D882
Modulus	2,000-2,100 MPa	ASTM D882
Thermal Properties		
Thermal Conductivity	0.20 W/m/K	ASTM C177
Glass Transition Temperature	-40.0˚C	ASTM D4065
Melting Temperature	162-168˚C	ASTM D3418
Electrical Properties		
Dielectric Constant at 1kHz	7.6	ASTM D150
Dielectric Strength at 1.0mm	20-25 kV/mm	ASTM D149

Although this introduced some stress relaxation, it was necessary to maintain constant strain during the Raman scan to achieve a predictable laser scatter.

2.2.3 Raman Spectroscopy

The Raman spectroscopy setup had a green Argon laser with a 532 nm wavelength, with the grating set at 600 BLZ = 500 nm for a center position of 2150 cm^{-1} and a range of 50 to 3800 cm^{-1}. Although this range was not necessary for the analysis of this study, it provided the best resolution for our peak analysis. The laser power was set to ~1 mW during testing. During Raman measurements, the CCD was cooled to liquid nitrogen temperature (-196 °C). All of our studies were set to perform three accumulations with a 15 s exposure time and at each applied strain state (see section 2.2.2) to ensure proper resolution of the Raman spectra.

2.2.4 In Situ Localized Strain Measurement

Video recording of the load tests was accomplished using a Keyence VHX-200 series digital microscope equipped with a VHX-J20 lens at 20× magnification. This setup enabled the collection of real-time AVI files at 60 fps during the mechanical loading of the PVDF thin film. It should be mentioned that the same MTS micro-load frame was employed and commanded to execute the same load profile used for the Raman spectroscopy test. A simple speckle pattern was implemented to allow for numerical analysis of the surface strain in the necking region. This allowed for the correlation between the strain distribution of the film and the measured Raman spectra at equal degrees of elongation. Since the comparison between surface strain distribution and the Raman spectra was done using the elongation and load, the pausing approach used for Raman collection was not implemented during the AVI file collection. Frame images were extracted, using MATLAB as post-processing software, and a digital image correlation (DIC) technique was also implemented using MATLAB.

2.3 Results and Discussions

2.3.1 Micro-Tensile Load Data

The PVDF film specimens were mechanically drawn using controlled monotonically increasing displacements of the load frame's crosshead. Four test cases were examined for repeatability purposes. The load frame was commanded to pause at 2.54 mm increments to allow for Raman measurements, as was discussed in section 2.2.4. The relationship between load and crosshead displacement for a representative set of tests is shown in

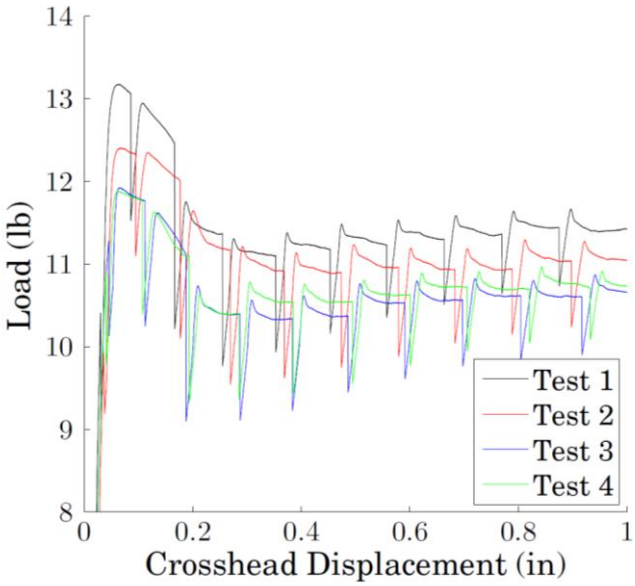

Figure 2.1 Loading curve showing pausing during displacement controlled loads to collect Raman data

Figure 2.1. From this representative plot, stress relaxation during the commanded pauses was evident. Upon restarting the crosshead displacement, the load recovered to a level nearly at which it was prior to the pause.

2.3.2 Raman Spectroscopy Data

The collection of Raman spectra to characterize the alpha phase and the beta phase was implemented in this study as a means of *in situ* monitoring. The Raman spectrum for alpha and beta phase is unique, as discussed in section 1.4.2.2 and shown in Figure 1.2. Previous studies conducted pre- and post-analysis using WAXD, FTIR, and Raman analysis, yet none of the researchers considered investigating the gradual transition of alpha to beta phase during mechanical loading [1-4]. Thus, the experiment discussed in section 2.2.2 was conducted for obtaining the Raman spectra of PVDF thin films under different levels of applied strains. This test required the laser to be pointed at the necking region during mechanical loading and that many scans be taken throughout the loading profile.

Typically, the removal of the background and any influence of fluorescence was done by fitting the data to Huber or Truncated Quadratic functions as proposed by Mazet et al. [5]. This allowed for a more interpretable signal in which peak wavenumbers were not absorbed by the residual Rayleigh scattering. In addition, by not using a traditional polynomial fit, the minimization of a non-quadratic cost function only required an order and threshold as input parameters, which reduced the effect of user-defined initial guesses. As determined by Mazet et al. [5] and illustrated in Figure 2.2, the asymmetric forms of the Huber and Truncated Quadratic functions best fit the lower

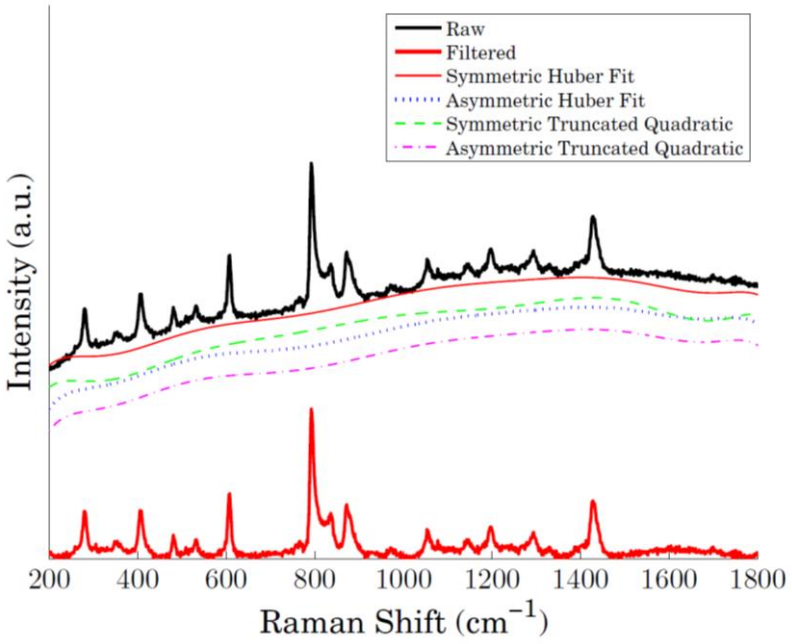

Figure 2.2: Background removal of the Raman spectra for more interpretable signal and analysis of peaks

bound of the Raman spectra. This approach has the additional benefit of accounting for Gaussian noise at small positive values of the spectra. Without the removal of background, fluorescence, and Gaussian noise, each spectrum displayed a trailing-off effect as observed in Figure 2.2. Since the severity of trailing-off differed from each set of data that was collected, it was difficult to compare the observed peaks and their actual intensity.

Previous research of Raman spectra characterization of PVDF identified that alpha and beta phase PVDF have distinct peaks at 794 cm^{-1} and 839 cm^{-1}, respectively. To monitor the progress of the phase transformation of PVDF during mechanical drawing, the relation between these two Raman peaks was examined using the ratio between the beta and alpha responses, as presented in equation 2.1.

$$\frac{\beta}{\alpha} = \frac{Intensity(\beta)}{Intensity(\alpha)} = \frac{Int.(RamanShift = 839cm^{-1})}{Int.(RamanShift = 794cm^{-1})} \tag{2.1}$$

This formula quantified that the film was predominately alpha for a ratio of less than 1 and predominantly, beta for a ratio of greater than 1. The phase transformation from alpha to beta as time and crosshead displacement increased is shown in Figure 2.3. It should be noted that increasing β/α ratio corresponded to increasing crosshead displacement and time. This corresponded with previous studies that had shown the transformation of PVDF from alpha to beta as the specimen plastically deformed [1, 2, 6]. For each stretch ratio, there were two Raman spectra

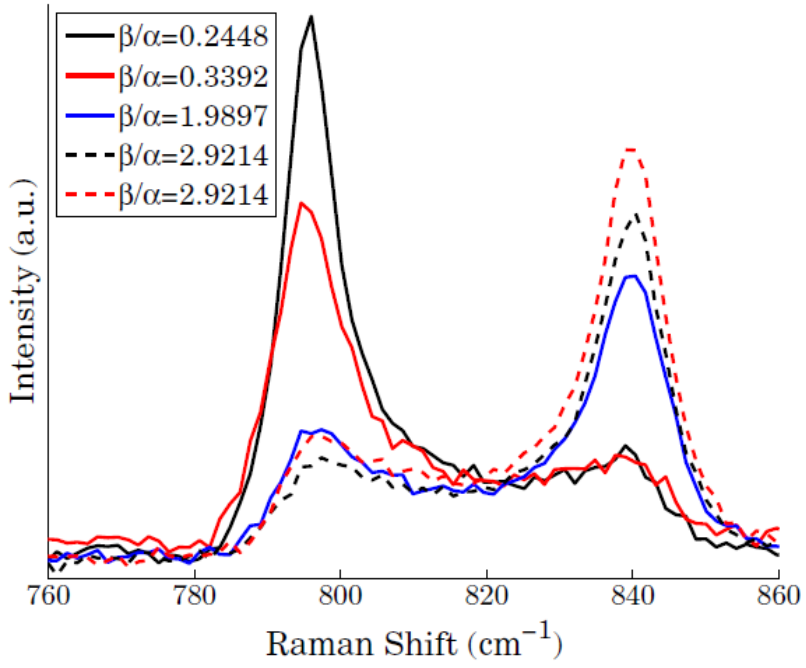

Figure 2.3: In Situ progression of alpha phase changing to beta phase during mechanical deformation

collected in order to account for stress relaxation that occurred in the thin film. After the sample was stretched and paused, as discussed in section 2.2.2, a Raman scan was collected immediately after the pause and again 30 s later before mechanical stretching was resumed. These 30 s allowed for the chain alignment to stabilize and a more consistent Raman scan to be produced, as shown in Figure 2.3.

2.3.3 Strain Data

To analyze the strain in the PVDF thin film, it was necessary to look at the local region in which necking occurred. Beta phase was produced in the localized areas of high strain as the stretching caused chain alignment. The beta phase was only produced in the regions of high strain as necking caused the transition from the spherulitic structure of alpha phase to the fibrillar structure of beta phase [7].

To measure the local strains within the plastic necking region, digital image correlation measurements were taken as described in section 2.2.4. The speckle pattern method is shown in Figure 2.4 at various times throughout the mechanical deformation. The speckle pattern shows that the strain distribution was not uniform on the surface of the PVDF thin film; namely, the necking region became apparent in Figure 2.4c-d. The load applied corresponding to each image in Figure 2.4a-i is shown in Figure 2.5. To numerically analyze this speckle pattern, an elliptical shape-fitting tool in MATLAB was used to calculate the elongation that occurred in 5 s intervals throughout the

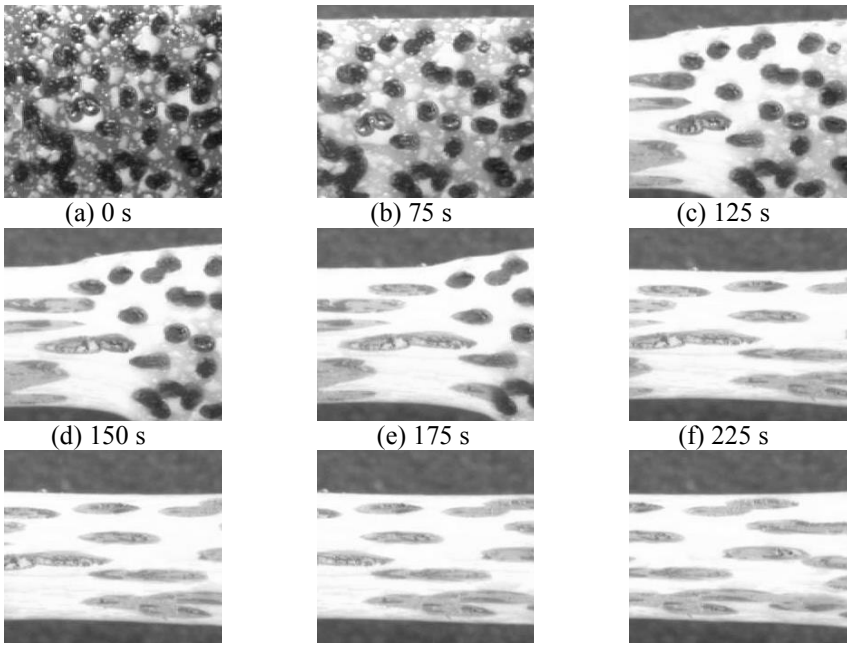

Figure 2.4: Time dependent strain images from DIC using micro-load frame while under Keyence microscope

duration of the test. The incremental values from each image were used to get a local strain in the necking region for every 5 s during the entire test. These values were correlated back to the applied load to provide a direct relationship between global load and local strain.

Specifically, DIC image analysis was carried out using the image processing toolbox in MATLAB. A region of interest (ROI) was defined on the image to narrow in on one particular "speckle." This was done on a few different speckles to ensure the minimal effect of user dependence. Once ROI was chosen, the image was transformed to a binary image based on a given threshold. From this step, MATLAB was programmed to fit the black speckle with an appropriate ellipse to determine the length of the major axis and the ellipse orientation. With these two values, the length of the ellipse was calculated along the axial direction and recorded for each image. It should be noted that ROI for each image was chosen to examine the same speckle progression throughout testing. This analysis is displayed in Figure 2.6.

This DIC analysis was implemented to obtain the local strain in PVDF specimens in a region where necking and drawing, resulting in plastic deformation, occurred during tensile loading. Necking is a mode of deformation during tensile testing where relatively large strains localize in a small region that was disproportionate to the global strains of the specimen. In addition, once necking occurred, a drawing phenomenon was observed.

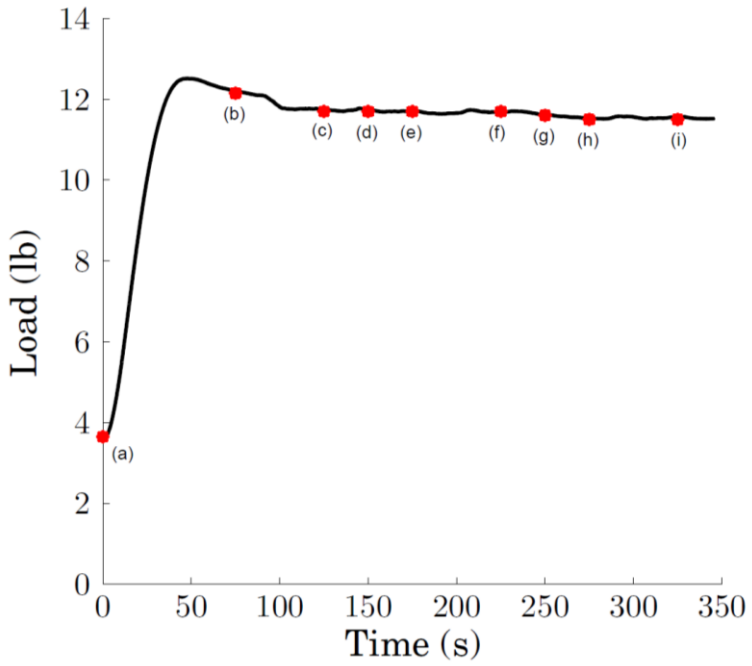

Figure 2.5: Loading curve corresponding to DIC images to show local strain image correlation to loading profile

Drawing is the resulting plastic deformation that propagated out from the necking region. This occurred due to the strengthened microstructure that formed in the necking region to cause the PVDF film to no longer strain in the reinforced region but to propagate out to the rest of the specimen. This necking phenomenon was what enabled the spherulites of the PVDF to break and form a more fibrillar morphology. The necking phenomenon resulted in a much stronger microstructure, which led the specimen to draw rather than break, because there was a larger breaking load required to fail the film within the stretched region [6].

As the strains within the necking region were highly localized, global strain was not used for calculating the correlation between mechanical elongation and phase transformation in localized areas. First, engineering strain was calculated on a global level, taking into account the initial area, length, and the overall load applied. The engineering stresses (σ_e) and strain (ε_e) values are described in equations 2.2-2.4:

$$\sigma_e = \frac{P}{A} \tag{2.2}$$

$$\varepsilon_e = \frac{\delta}{L} \tag{2.3}$$

$$\sigma_e = E\varepsilon_e \tag{2.4}$$

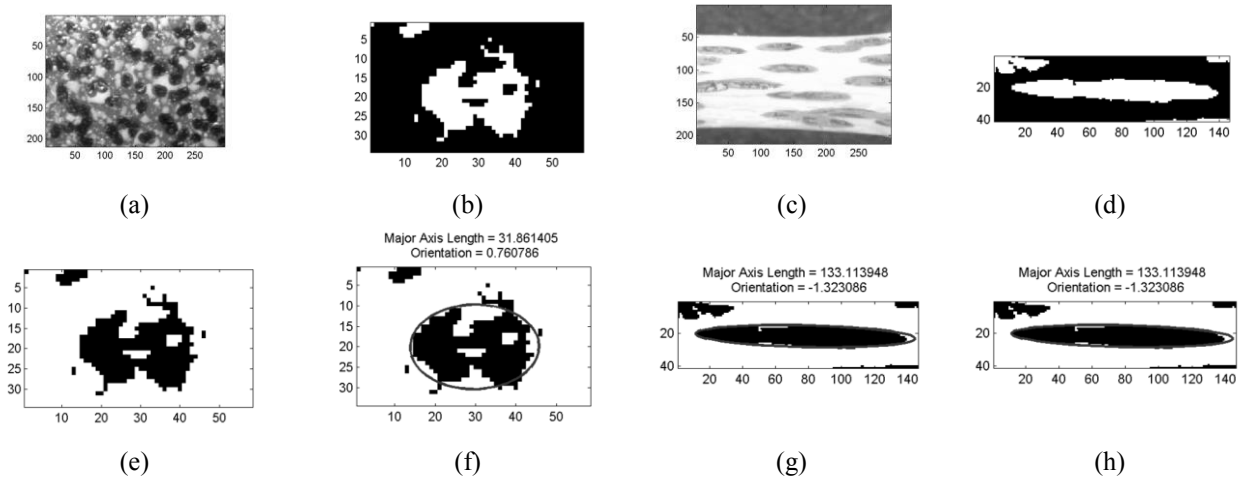

(a) (b) (c) (d)

(e) (f) (g) (h)

Figure 2.6: Images used in image processing toolbox in MATLAB to obtain axial deformation from a fit ellipse

Where P is the load applied, A is the global area of the gage, δ is the change in gage length, L is the original gage length, and E is the elastic modulus of the material. In this scenario, the usefulness of engineering stress and strain was limited due to the nonlinear behavior that occurred after the formation of the necking region. Once a necking region developed due to yielding in the material, equation 2.4 was no longer valid as Young's modulus was no longer constant. This led to the necessity of an incremental analysis as shown below in equation 2.5:

$$d\varepsilon_t = \frac{dL}{l} \rightarrow \varepsilon_t = \int_{l_o}^{l} \frac{1}{L} dL = \ln(\frac{L}{L_o}) \tag{2.5}$$

This incremental strain could be looked at for a local region of the specimen, thus allowing for the analysis of the local strain in the necking region, in the necking-drawing region, or in the outside region as shown by the time-dependent strain images in Figure 2.4.

In addition, to compare the results obtained in this study to similar results obtained by Mohammadi et al. [8], it was useful to define the following variable, λ, which is the extension ratio or stretch ratio, as shown in equation 2.6.

$$\lambda = \frac{L}{L_o} \tag{2.6}$$

This logarithmic scaled variable allowed for local strain data to be presented on a logarithmic-scale plot for direct comparison to existing literature. It should be noted that, by defining the extension ratio as such, the original sample stretch ratio prior to mechanical loading would be "1," which is observed in Figure 2.7.

2.3.4 Correlation between Raman Spectra Data and Strain Data

To correlate the data collected during the Raman scans to the data obtained during the DIC strain analysis, the applied load was used. The Raman spectra were collected independent of the strain analysis since the Raman microscope could not be used in conjunction with the Keyence microscope. In addition, the Raman scan required that the micro-load frame be paused to collect data, as described in Section 2.3.2, whereas the Keyence microscope allowed for an AVI file to be collected in real-time for later post-processing of the evolution of the surface ellipses, as described in section 2.2.4. To correlate the two sets of data, the load observed from the PVDF was used, and the data was fit with a polynomial trend line to obtain a strain corresponding to load and a β/α corresponding to load. By making a relation between load and strain from the load frame and AVI data, and load and β/α from the Raman spectra data, it was possible to give a specific relative intensity relating to strain as shown in Figure 2.7. All four test cases are shown in Figure 2.7 for repeatability purposes.

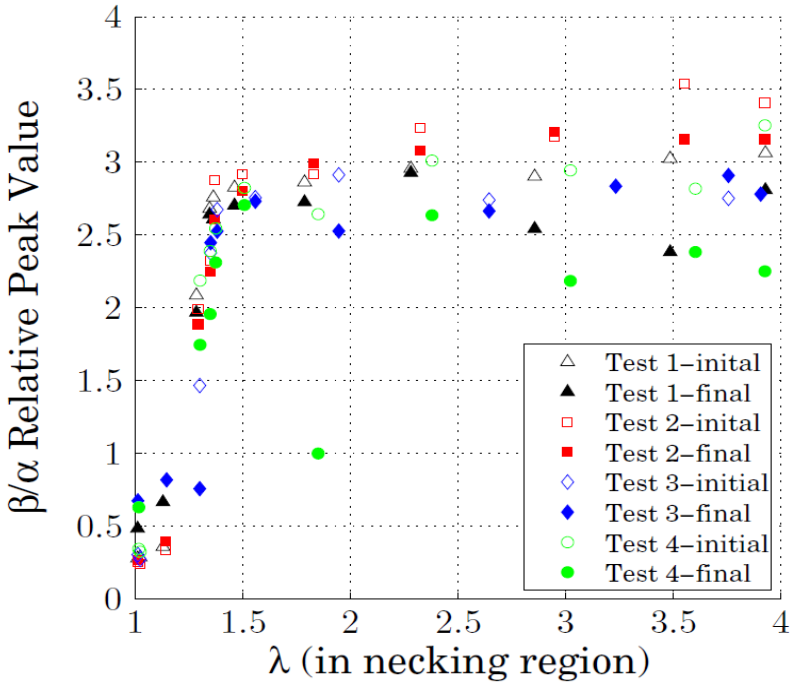

Figure 2.7: Correlation between strain image and Raman spectra to relate stretch ratio in necking region to beta phase content, where initial scans are taken immediately after pause and final scans are taken 30 s after pause

From the correlation between stretch ratio and beta content in PVDF, it can be seen in Figure 2.7 that there was a near-linear increase in beta content from a stretch ratio of 1 to just below 1.5. After a stretch ratio of 1.5, the conversion to beta content plateaued at about a relative peak ratio of 3. This is important, because only a stretching ratio of 1.5 was necessary to maximize beta content. In addition, this trend held for Raman measurements taken at the beginning and end of each 30 s pause of the load frame, as discussed in section 2.2.2. The Raman scans corresponding to the spectra collected immediately after the pauses are shown by the hollow markers in figure 8. The Raman data collected 30 s after the pause appeared to be slightly lower in most cases, due to stress relaxation of the polymer chains. This result is shown by the solid markers in Figure 2.7.

These results could be compared to existing literature such as work presented by Mohammadi et al. [8] in which the stretch rate and initial and final stretch ratios are the values of interest. Mohammadi et al. [8] reported that the stretch ratio required for the beta phase content to plateau was 5. This differs from the results presented here and may be due to the FTIR method used to calculated beta phase content. Also, for the strain rate studied here (*i.e.*, 5.08 $mm \cdot min^{-1}$), there was no strain rate dependence [1].

2.4 Conclusions

During mechanical stretching of PVDF thin films, Raman spectroscopy and digital image correlation were used to analyze the phase transformation of PVDF from alpha to beta phases. During the mechanical deformation of freestanding thin films, the Raman spectra in the necking region of the PVDF were collected to calculate the molecular chain alignment in the polymer. In addition, DIC was performed during mechanical deformation to determine the local strain in the areas of phase transformation (and stretching/necking). As a result, the local strain or stretch ratio was determined *in situ* that resulted in this phase transformation. This allows for characterization of future PVDF thin films by understanding the minimum stretch ratio needed to yield maximum phase transformation from alpha phase to beta phase of PVDF.

Chapter 2: References

1. Constantino, C.J.L., et al., *Phase Transition in Poly(vinylidene fluoride) Investigate with Micro-Raman Spectroscopy.* Applied Spectroscopy, 2005. **59**(3): p. 275-279.
2. Constantino, C.J.L., et al., *The Investigation of alpha to beta Phase Transition in Poly(Vinylidene) Fluoride (PVDF).* Electrets ISE-12 12th International Symposium, 2005: p. 178-181.
3. Matsushige, K., et al., *The II-I crystal transformation of poly(vinylidene fluoride) under tensile and compressional stresses.* Polymer Journal, 1979. **21**: p. 1391-1397.
4. Salimi, A. and A.A. Yousefi, *FTIR Studies of beta-phase crystal formation in stretched PVDF films.* Polymer Science Direct, 2003. **22**: p. 699-704.
5. Mazet, V., et al., *Background removal from spectra by designing and minimising a non-quadratic cost function.* Chemometrics and Intelligent Laboratory Systems, 2005. **76**: p. 121-133.
6. Jain, A., et al., *Detailed studies on the formation of piezoelectric beta-phase of PVDF at different hot-stretching conditions.* Sensors and Smart Structures Technologies for Civil, Mechanical, and Aerospace Systems, Proc. of SPIE, 2010. **7647**: p. 2C-1-2C-11.
7. Perkins, S., *Hypervelocity Impact Detection: An Investigation into Piezoelectric Response of PVDF Thin Films*. 2010, University of Kent.
8. Mohammadi, B., A.A. Yousefi, and S.M. Bellah, *Effect of tensile strain rate and elongation on crystalline structure and piezoelectric properties of PVDF thin films.* Polymer Science Direct, 2007. **26**: p. 42-50.

Chapter 3: Concurrent Phase Change and Polarization of PVDF Thin Films using High-Temperature and High-Voltage Setup

3.1 Introduction

The development of a spray-deposited piezoelectric impact detection sensor is desired for use in civil, military, and aerospace applications, among others. Polyvinylidene fluoride (PVDF) is ideal for this purpose due to its flexibility, resistance to creep, and mechanical robustness. In addition, PVDF-based coatings can be designed to be easily deposited on large-scale complex-geometry structures. To enable a PVDF-based thin film sensor for large structures, the phase change and polarization of the PVDF must occur after the conformal deposition of the film onto the structure. In the previous chapter, mechanical stretching was utilized to induce the phase change of the PVDF, which is not feasible when applying such a sensor onto an airplane or bridge. To overcome this shortcoming, phase transition due to elevated temperature and high voltage will be investigated. This will allow for in situ sensor fabrication, which is ideal for the implementation of a conformal sensor for structural health monitoring applications.

Currently, the voltage and temperature parameters reported in the literature vary widely, which necessitates a full characterization of this parameter space for the actuation of the desired phase transformation. For example, authors such as Kim et al. [2] used 1.5 MV/cm in an enclosure at 100 ˚C for approximately 30 min when poling an already stretched blend of PVDF and MWCNT using a dielectric poling setup. Additionally, authors such as Chan et al. [3] used 0.3 MV/cm in an enclosure at 105 ˚C for approximately 2 h when Corona poling annealed and hot-pressed thin films made of a PVDF-TrFE copolymer blend. In addition, Chan et al. [3] implemented a setup that required multiple poling and cooling steps in order to obtain a piezoelectric sample. In a thesis by Stroyan [4] pure PVDF, a PVDF-TrFE copolymer and a PVDF-TrFE-PZT composite was phase changed and poled using poling fields around 0.4 MV/cm at ambient and raised temperatures to investigate peak polarizations. Lastly, Esterly [5]

concludes in his thesis that shorter poling times are required for samples at higher temperatures, whereas longer poling times are required for samples at lower temperatures. The variations in the referenced literature are the motivation of a further investigation into the effect of high voltage and high temperature on the phase transformation from alpha to beta phase of PVDF. This research focuses on the concurrent phase change activation and polarization of spray-deposited PVDF-based coatings using a high-temperature enclosure in conjunction with a high-voltage setup. Electrodes were placed on either side of the sample and inserted into an oven with temperatures ranging from 60 ˚C to 150 ˚C, while a voltage ranging from approximately 0.04 MV/cm to 0.4 MV/cm was applied to the sample. Phase change characterization of the coatings was done with a Raman spectroscopy setup using an Argon ion laser at a wavelength of 532 nm.

3.2 Experimental Methodology

3.2.1 Specimen Fabrication

Sample preparation focused on placing plate electrodes on either side of the PVDF samples. To check for phase change activation after applying high voltages and high temperatures, it was necessary to have a top electrode that did not interfere with the Raman spectroscopy measurements. In order to achieve this, indium tin oxide (ITO) was e-beam deposited on the top of the samples. Depending on the sample type, the bottom electrode used was either electrically conductive tape or an aluminum substrate.

3.2.1.1 PVDF Thin Film Specimen

In order to establish the phase transition performance of a neat PVDF thin film, a sheet of PVDF was purchased from McMaster-Carr, which was produced from Solef resin grade 9009. The complete material properties for this film are listed in Chapter 2, Section 2.2.2. However, in this chapter, the film thickness used was 0.127 mm, as compared to the 0.254 mm film used in Chapter 2. A thinner PVDF thin film allowed for lower applied voltages across the PVDF to achieve the necessary voltage gradient range for comparison to other research in the literature. The PVDF thin film specimens were cut to dimensions of 25.4 mm x 76.2 mm.

In order to expose areas of the thin films to an electrical voltage while exposing the specimen to high temperatures, plate electrodes were applied to either side of the specimen, as shown in Figure 3.1. The top electrode was made of ITO which is a transparent metal-oxide that would not interfere with the Raman measurement. Section

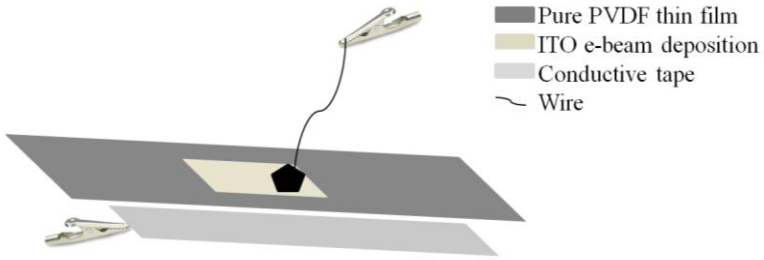

Figure 3.1: Schematic of poling setup for PVDF thin film

3.2.1.3 gives a thorough explanation of the deposition process of the ITO, as well as the Raman response of the ITO over PVDF. The bottom electrode was a piece of conductive tape. In order to electrically connect to the specimens, wires were attached to the top ITO electrode using Hysol TRA-DUCT 2902 silver-filled epoxy. This silver-filled epoxy was useful since it could cure at room temperature and is highly conductive. Although exposure to heat could be used to expedite the curing process, it was not desired to expose the sample to additional heat without some voltage applied. In addition, a lead wire was connected to the bottom electrode by utilizing an alligator clip to attach directly to the conductive tape.

3.2.1.2 Kynar Aquatec PVDF-Based Paint Specimen

In order to develop an easy-to-deposit thin film over large areas, a PVDF-based latex paint was utilized. The base for this paint was obtained from Arkema in the form of Kynar Aquatec, an emulsion of PVDF/acrylate nanoparticles with a diameter of 110 nm. This base solution was designed to be used as an architectural coating for roofs, sidings, windows, and various other construction applications. The Kynar Aquatec paint was combined with commercial off the shelf (COTS) additives to achieve a spray-deposited uniform thin film that could be used in sensing applications. The specific constituent concentrations are still considered proprietary at this point. The formulation focused on a uniform sprayable thin film with an approximate thickness of 65 μm to 75 μm, to properly adhere to surfaces for use as a sprayable sensor on complex geometries. Upon mixing, the paint was put into a high-volume-low-pressure (HVLP) spray gun from Anest Iwata, model LPH101 with gravity feed and low volume technology. The paint was applied in two coats with a 30 min drying time between each coat. Each coat consisted of two passes from the spray-gun, where the first pass was applied from left to right and the second pass was applied from top to bottom.

The PVDF-based sprayable paint was deposited onto an aluminum substrate to be used as the bottom electrode. The aluminum substrate used was aluminum alloy 6061 purchased from McMaster-Carr with a thickness

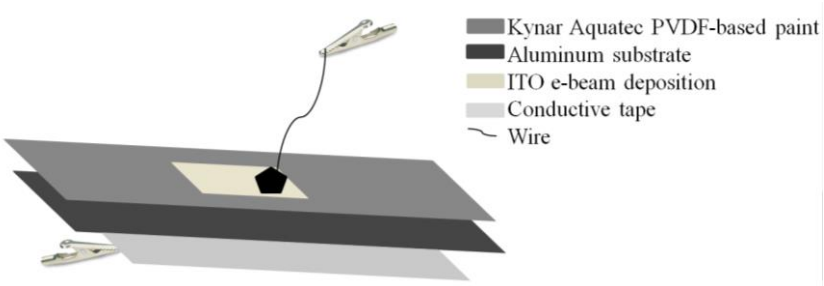

Figure 3.2: Schematic of poling setup for Kynar Aquatec PVDF-based sprayable paint

of 0.3175 cm and a polished mirror finish. To connect the voltage source to the aluminum substrate for current to pass through, a small piece of conductive tape was attached to the metal, and alligator clips were attached to the tape as shown in Figure 3.2. The conductive tape initially used was 3M Fabric Tape CN-3190, which has nickel on copper-plated polyester fabric. This tape is listed as an electrically conductive tape, but it was later determined that the adhesive on this tape may not be conductive. In order to remove any issues of the non-conductive adhesive, 3M copper-coated polyester cloth tape X-7001 was used, which contains conductive acrylic adhesive on both sides of the tape. As with the sheet PVDF thin film, a top electrode of ITO was deposited onto the PVDF paint. This electrode was also connected to a wire lead using the TRA-DUCT 2902 silver epoxy.

3.2.1.3 Indium Tin Oxide Electrode Deposition

For the thin films to have a top electrode that did not interfere with Raman spectroscopy, ITO was deposited on top of the PVDF thin films using an electron beam (E-beam) deposition technique. E-beam deposition of ITO is fairly common and was successfully accomplished by authors such as Fallah et al. [6] and Wang et al. [7]. The desired electrode area measured approximately 1.27 cm x 0.635 cm and was masked using non-conductive Kapton tape due to its high temperature tolerance without gas release. The deposition rate used for depositing the ITO was set at 0.3 Å/s for approximately 720 s for a total thickness of about 200 Å. The thickness of the ITO was confirmed on a reference substrate using scanning electron microscopy (SEM) as shown in Figure 3.3.

To ensure that ITO deposition did not interfere with the alpha and beta characteristic peaks in the Raman spectra, scans were collected with an ITO film thickness of 100 Å and 200 Å and are shown in Figure 3.4. Although the spectra appear to vary slightly in magnitude at the alpha and beta representative peaks, the relative peak values as defined by Riosbaas et al. [8] are consistent between the three Raman spectra shown.

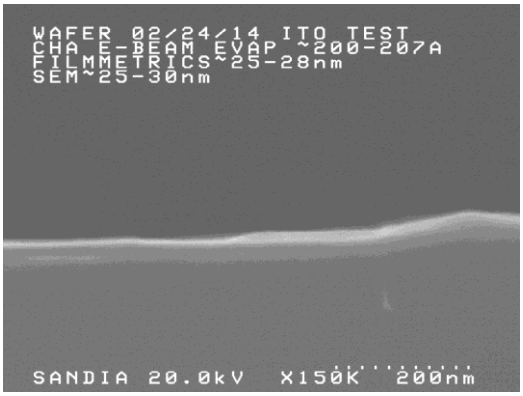

Figure 3.3: SEM image of ITO on reference substrate confirming thickness of ITO using E-beam deposition

3.2.2 High Voltage and High Temperature Exposure

In order to expose the specimens to elevated temperatures while applying a high voltage across the PVDF, a combined oven and power supply setup was implemented. The oven used for raising the temperature of the PVDF thin films during poling was a VWR 414005-108 gravity convection oven with exhaust ducts on the top for the wiring of the voltage supply to feed through. The oven was capable of reaching temperatures up to 230 ˚C with fluctuations of ±0.6 ˚C and variations of about ±2.7 ˚C at 150 ˚C. As PVDF has a melting temperature of ~170 ºC,

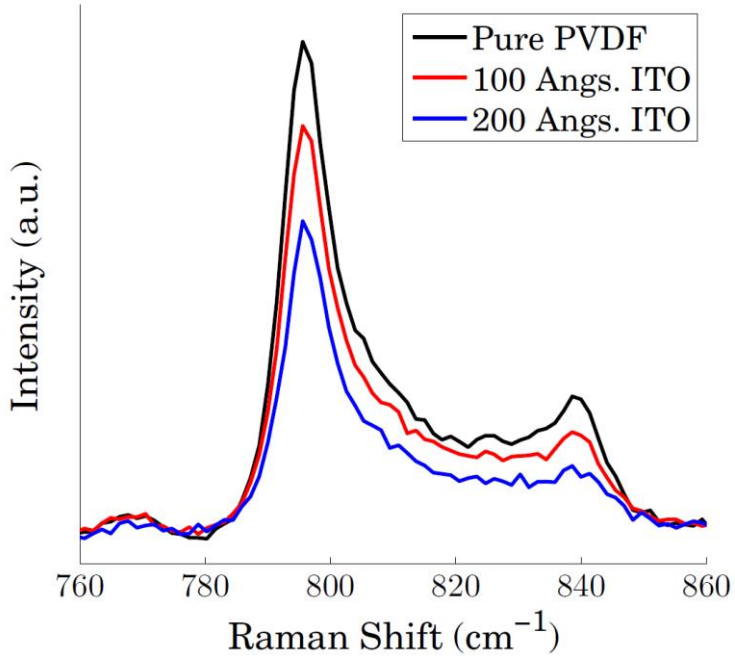

Figure 3.4: Plot of pure PVDF thin film surface compared to that with 100 Å and 200 Å of ITO

the oven temperatures were kept significantly lower than that. The Curie temperature of pure PVDF is 150 ºC, and the recommendation from the literature was to keep the poling temperatures right around that of the Curie temperature [5, 9].

After the specimens were heated to the specified temperature, the power supply was used to place a high voltage across the specimens. The voltage source used was a Stanford Research Systems high voltage power supply series PS325 capable of voltages ranging from 25 V to 2500 V and a maximum output current of 10 mA. The voltage source capabilities were calculated as voltage gradients for a direct comparison between varied thickness samples. The highest voltage gradient applied to the PVDF thin films was approximately 0.2 MV/cm whereas the highest voltage gradient applied to the Kynar Aquatec PVDF-based thin film was approximately 0.35 MV/cm. This voltage source also retains the ability to set a trip current to reduce the current passed through the sample if dielectric breakdown occurs. Due to the thin nature of the films as well as their low resistivity, currents on the order of microamps were sufficient for our testing purposes. Thus, the trip current was typically set at about 1 mA and was only tripped if dielectric breakdown occurred causing the electrical charge to flow freely through the material.

The neat PVDF sheet was characterized first by varying the parameters of voltage, temperature, and voltage duration. The temperatures that the thin films were tested at ranged from 60 ºC to 150 ºC. Initially, the voltages that the thin films were subjected to were 1.1 kV to 2.5 kV, but as the results continued to show no phase change occurring, the voltage was kept at 2.5 kV while temperature and duration were varied. Finally, the duration for which the specimens were exposed to the high voltage was from 10 minutes to 180 minutes. The lower duration exposures were due to results from previous research, which was thought to be relevant to this work [1-3, 10, 11]. The fact that the equipment available limited the voltage gradients of 0.197MV/cm (lower than some of the reports in the literature by 10 fold), a relation between the voltage applied and the duration it was applied for was defined.

The voltage and duration exposures of all of the successful reports in the literature were compiled and are shown in Table 3.1, and a calculation was performed to obtain the product of the voltage gradient and duration of exposure. Using this value, the voltage gradient limitation from the available equipment (0.197 MV/cm) was used to identify the desirable range of durations for further experiments. Equation 3.1 gives the mathematical representation for this process where t is the time duration of exposure, ∇V is the voltage gradient, superscript R refers to the reported values, and superscript E refers to the experimental values used in this work. A maximum duration of 210 minutes was determined, and thus established the duration range of the experiments.

$$t_D^E = \frac{t_D^R \nabla V^R}{\nabla V^E} \tag{3.1}$$

The experiments involving the Kynar Aquatec films were originally supposed to follow those of the neat PVDF thin films. However, due to dielectric breakdown, a modification of approach was taken to only look for the dielectric breakdown of the thin films and then examine the Raman spectra for the thin films at the dielectric breakdown, as that was the maximum voltage that could be achieved. As will be discussed, the void content in the films led to poor dielectric breakdown properties. To overcome this, a thin film and temperature was chosen, starting at room temperature and working upwards. The applied voltage was ramped at 100 V increments until breakdown occurred or when the power supply maxed out at 2.5 kV. For the next specimen, the temperature was increased and the voltage ramp procedure was performed again.

3.3 Results and Discussions

3.3.1 PVDF Thin Film Exposed to High Temperature and High Voltage

First, an investigation of the potential to phase change and pole neat PVDF was performed. Numerous measurements were taken for phase change, including parameters such as temperature, voltage, and duration of

Table 3.1: Voltage and temperature exposure to pure Kynar Aquatec PVDF-based paint

Author	Sample	Voltage Gradient (MV/cm)	Temperature (ºC)	Duration (m)	Additional details
Mohammadi et al. [1]	Pre-streched, pure PVDF thin films	1.8	103	10	The voltage gradient was applied for 10 m at temperature, and continued during cooling to ambient temperature
Kim et al. [2]	Drawn neat PVDF film	1.5	100	30	N/A
Kim et al. [2]	Drawn PVDF/MWCNT nanocomposite film	1.5	100	30	Contains carbon nanotubes which can greatly affect the poling outcome
Chan et al. [3]	Thick PVDF-TrFE films	0.26-0.3	100-120	60-240	Various combinations of temperature and times are investigated with two different Corona poling setups

voltage exposure. Unfortunately, even at 2.5 kV, it was found that for 3 h of applying the voltages at temperatures up to 150 ºC, there was no phase change observed in the PVDF thin film.

The Raman spectra were collected after exposure to high temperature and high voltage and a representative set of spectra are shown in Figure 3.5. In Figure 3.5, the black line corresponds to the Raman spectra obtained outside of the ITO electrode region where the sample should not have been exposed to any voltages (since there was no top or bottom electrode at that point). The red and blue lines both correspond to the same ITO electrode, where scans were taken at two different points to investigate if the phase change had occurred at any point. It is important to note that these spectra were collected at random points within the ITO electrode area. Multiple scans were collected for confirmation of no phase change in the area of the ITO electrode.

3.3.2 Kynar Aquatec PVDF-Based Paint Exposed to High Temperature and High Voltage

Despite the lack of ability to phase change and pole the neat PVDF thin films, it was thought that the much thinner spray-deposited PVDF thin films would allow for high enough voltage gradients to induce a phase change. Samples of the Kynar Aquatec PVDF-based latex paint were initially investigated as sprayed on an aluminum substrate with e-beam deposited ITO as the top electrode. It was quickly found that these films were very thin (approximately 66 μm) on the substrate and were quick to break down, especially at higher temperatures. Initially,

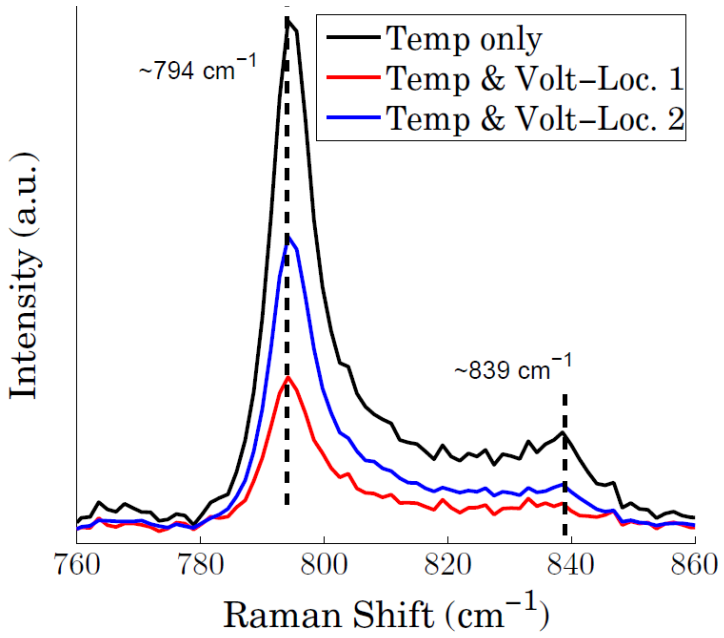

Figure 3.5: Plot of pure PVDF thin film tested at 2.5 kV at 135 ºC for 180 min.

the voltage was brought immediately to the desired voltage, but this yielded immediate breakdown. As discussed in Section 1.4.4, dielectric breakdown occurs when a maximum voltage is applied that collapses the dipoles and allows electrons to flow freely between the electrodes. Due to breakdown of numerous films, initial plans to test the films up to temperatures of 150 ºC were abandoned. These specimens were all started at a voltage of 100 V and the voltage was increased in 100 V increments until breakdown was achieved or 2.5 kV was reached. The results of these tests are presented in Table 3.2.

It is suspected that dielectric breakdown could be occurring for a variety of reasons. For example, the thin films are not completely homogeneous and do contain various pores that are visible to the naked eye. These pores are also known as air pockets and have a dielectric breakdown of 0.03 MV/cm compared to that of pure PVDF, which has a dielectric breakdown of 7.7 MV/cm [12, 13]. This drastic difference causes issues whenever there are air pockets observed in the material. In addition, it is unknown if each of the COTS additives included in the paint play a small or large role in the dielectric breakdown of the sample.

As shown in Figure 3.6, there were no changes observed after exposure to a high voltage at room temperature in the Kynar Aquatec PVDF-based latex paint, even when voltages up to 2.5 kV (approximately 0.379 MV/cm) were applied. Although the peaks observed in Figure 3.6 do appear to vary in magnitude, the relative beta/alpha peak as described in detail in section 2.3.2, equation 2.1 is similar for both spectra. This is indicated by a lack of a significant change in Raman peak at 839 cm^{-1}. When the voltages were applied in very small increments, the sample was able to handle voltages up to 2.5 kV at a temperature of 23 ˚C. Figure 3.6 was collected to show that no phase change occurred when high voltages were applied while the samples were at room temperature. Due to the fact that the Kynar Aquatec PVDF-based latex paint could not sustain high voltages being applied at higher temperatures, it is not unusual that the paint could not undergo a phase change.

Table 3.2: Voltage and temperature exposure to pure Kynar Aquatec PVDF-based paint

	Breakdown Voltage	**Temperature**
Sample 1	2.5 kV (0.379 MV/cm)	23 ºC
Sample 2	2.2 kV (0.333 MV/cm)	50 ˚C
Sample 3	1.9 kV (0.288 MV/cm)	58 ˚C
Sample 4	1.6 kV (0.242 MV/cm)	75 ˚C

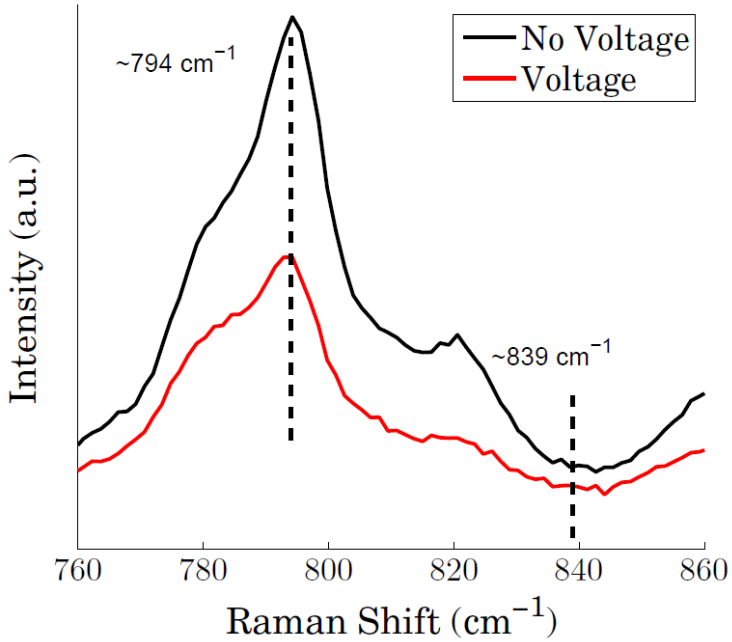

Figure 3.6: Kynar Aquatec PVDF-based latex paint before and after exposure to 2.5 kV at 23 ºC

3.4 Conclusions

In this chapter, an attempt was made to induce a phase change from alpha phase to beta phase PVDF through the application of concurrent high voltage and high temperature. First, the characterization was performed on the pure PVDF thin film as a baseline. Then, a sprayable Kynar Aquatec PVDF-based latex paint film was examined. It was found that the pure PVDF thin film was too thick to induce a phase change with the voltage supply available at this point.

It was found that the Kynar Aquatec PVDF-based paint could not sustain large voltages when applied at high temperatures without dielectric breakdown. The paint was able to sustain a maximum voltage of 2.5 kV (approximately 0.379 MV/cm) if applied at 0.1 kV (approximately 0.015 MV/cm) increments at room temperature (approximately 23 ˚C). This is unfortunate, as we were unable to induce any phase changes or polarization solely with the application of high temperatures and high voltages. It is believed that if the films were pre-stretched to induce a phase change, our setup could pole the thin films to obtain piezoelectricity. However, pre-stretching would remove the capability of scaling up to large complex-geometry structures. Therefore, this avenue was not explored any further.

Chapter 3 References:

1. Mohammadi, B., A.A. Yousefi, and S.M. Bellah, *Effect of tensile strain rate and elongation on crystalline structure and piezoelectric properties of PVDF thin films.* Polymer Science Direct, 2007. **26**: p. 42-50.
2. Kim, G.H., S.M. Hong, and Y. Seo, *Piezoelectric properties of poly(vinylidene fluoride) and carbon nanotube blends: beta-phase development.* Physical Chemistry Chemical Physics, 2009. **11**: p. 10506-10512.
3. Chan, H.L.W., et al., *Polarization of thick polyvinylidene fluoride/trifluoroethylene copolymer films.* Journal of Applied Physics, 1996. **80**(7): p. 3982-3991.
4. Stroyan, J.J., *Processing and Characterization of PVDF, PVDF-TrFE, and PVDF,-TrFE-PZT Composites*, in *Materials Science Engineering*. 2004, Washington State University
5. Esterly, D.M., *Manufactruing of Poly(vinylidene fluoride) and Evaluation of its Mechanical Properties*, in *Materials Science and Engineering*. 2002, Virginia Polytechnic Institute and State University: Blacksburg, Virginia.
6. Fallah, H.R., M. Ghasemi, and A. Hassanzadeh, *The effect of annealing on structural, electrical and optical properties of nanostructured ITO films prepared by e-beam evaporation.* Materials Research Bulletin, 2007. **42**: p. 487-496.
7. Wang, R.X., et al., *Properties of ITO thin films deposited on amorphous and crystalline substrates with e-beam evaporation.* Semiconductor Science and Technology, 2004. **19**: p. 695-698.
8. Riosbaas, M.T., et al. *In situ phase change characterization of PVDF thin films using Raman spectroscopy*. in *Sensors and Smart Structures Technologies for Civil, Mechanical, and Aerospace Systems*. 2014.
9. Lovinger, A.J., et al., *On the Curie temperature of poly(vinylidene fluoride).* Macromolecules, 1986. **19**(5): p. 1491-1494.
10. Chan, H.L.W., P.K.L. Ng, and C.L. Choy, *Effect of poling procedure on the properties of lead zirconate titanate/vinylidene fluoride-trifluoroethylene composites.* Applied Physics Letters, 1999. **74**(20): p. 3029-3031.
11. Egusa, S. and N. Iwasawa, *Poling Characteristics of PZT/Epoxy Piezoelectric Paints.* Ferroelectrics, 1993. **145**: p. 45-60.

Chapter 4: Phase Change of PVDF-based Thin Films Using OMS and DMAc Casting

4.1 Introduction

The development of a spray-deposited piezoelectric impact detection sensor is desirable for applications such as aerospace, civil, and military structures. By formulating a paint that is piezoelectric, scaling up the size of the sensor becomes more realistic for industrial use. Polyvinylidene fluoride (PVDF)-based architectural coatings currently exist, where the PVDF is in alpha phase. In addition, some formulations exist where the paint is piezoelectric due to additional additives that are piezoelectric themselves (*i.e.* MWCNT and PZT) [1-4] . By formulating a piezoelectric paint without these additives there are fewer issues related to non-homogeneity in the paint. Current architectural paints exist exhibiting alpha phase PVDF molecular structure with no piezoelectric properties. However, these paints have excellent adhesion and flexural properties that would be useful in piezoelectric sensing applications. The early stages of this research placed emphasis on using these PVDF-based architectural coatings as piezoelectric sensors for structures by formulating some mixture that would exhibit beta phase characteristics and thus be polarizable. Initial experiments utilized the previously characterized PVDF thin film purchased from McMaster-Carr for a baseline characterization. To move towards the development of a spray-deposited thin film, the addition of a polar solvent dimethyl acetamide (DMAc) and organically modified silicate (OMS) particles were combined with PVDF solutions to attempt to cause a chemical-derived phase change of the PVDF. This chapter outlines this approach and the resulting changes to the PVDF structure.

4.2 Experimental Methodology

4.2.1 Sample Fabrication

Sample preparation focused on producing thin films with various chemical formulations to check for alpha to beta phase transition. The samples incorporated different weight percentages of various components to analyze

the phase change transition as well as feasibility as a thin film. To check for phase change activation, FTIR spectra were collected upon casting the thin films.

4.2.1.1 Kynar Resin Suspended in DMAc

A pure PVDF powder form resin was obtained from Arkema. This resin is labeled as PVDF Kynar resin and is most commonly used as a coating in the architectural industry due to its well-recognized resistance to temperature, radiation, and some environmental conditions that it may come into contact with. In addition, it can be processed at room temperature.

To first study the effect of pure PVDF Kynar resin suspended in the polar solvent DMAc, a basic formulation was made with four different weight percentages of Kynar resin as shown in Table 4.1. The solutions were prepared in a glass vial and placed into a Cole-Parmer brand water bath sonicator model 8850, capable of 50-60 Hz at a voltage of 117 volts and 0.7 amps. The vials were sonicated for 5 min to achieve dispersion of the powder in the solvent. Using a pipette, drops were placed onto glass substrates cleaned with acetone and rinsed using distilled water prior to drying with compressed nitrogen. These glass substrates were placed into the oven and baked at 70 ˚C for a minimum of 45 min, or until the solvent was completely dried out.

4.2.1.2 Kynar Resin Suspended in DMAc for Film Thickness Study

The thickness of the thin film can play a role in the drying time necessary for complete solvent evaporation. As such, it can also impact the surface adhesion for the thin film to the substrate as well as the brittleness of the film. In order to study the effect of the thickness of the thin film, another batch of Kynar resin suspended in DMAc was produced. This sample was formulated using the constituent amounts specified in Table 4.2. To ensure dispersion of the Kynar resin in the solvent, the solution was placed in the LabRAM mixer from Resodyn Acoustic Mixers at 40 % intensity at a speed of 60 Hz for a total of 30 s. Following mixing, the solution was placed into the water bath sonicator at ambient temperature for 5 min. The solutions were then pipetted in 700 μL increments onto a polished

Table 4.1: Weights of PVDF Kynar resin in various concentrations of 1 mL DMAc, prior to baking out

	Kynar (g)	PVDF Weight %
KYN1	0.1105	11
KYN2	0.2084	19
KYN3	0.3124	26
KYN4	0.4064	32

Table 4.2: Samples used to create definite volume thin film on polished aluminum substrate for film thickness study

	Kynar (g)	DMAc (mL/g)
KyDM-1	0.8027	4/3.6512
KyDM-2	0.8263	4/3.4642

aluminum substrate from McMaster Carr that measured 2.54 cm x 5.08 cm. This resulted in an approximate film thickness of 542.5 μm. Since this is quite thick for a thin film, it would require high voltages for polarizing. Therefore, another sample was prepared with 100 μL of solution on the same area substrate resulting in an approximate film thickness of 77.5 μm.

4.2.1.3 Kynar Resin and OMS Suspended in DMAc

The organically modified silicate (OMS) used was obtained from Nanocor. Their product is known as I.30E which uses a nanoclay surface treated with octadecyl ammonium by 28-32 weight % to produce a nanoclay that can improve the mechanical properties and solvent resistance of epoxy in room-temperature cured epoxy resin systems. The OMS came in powder form and appeared as an off-white or cream color.

Following the work performed by Buckley et al. [5], OMS was introduced into the mixture of PVDF and DMAc to attempt to obtain chemically-achieved PVDF phase change. Different weight-percentages of OMS were incorporated into the PVDF solution to determine if a critical amount of OMS was needed to achieve the desired phase change. To prepare the PVDF and OMS mixtures for FTIR measurement, the following procedure was implemented: (1) measure Kynar powder and OMS powder in the amounts specified in Table 4.3, (2) add associated amount of DMAc, (3) swirl by hand to cover powder with solvent, (4) place in water bath sonicator for 5 min, (5) deposit solution onto cleaned microscope. At this point, there were two drying methods used on each sample. One set of specimens were placed in the oven and baked at 60˚ C for a minimum of 45 min or until the solvent had completely evaporated out. In addition, another set of specimens were placed on a slide and allowed to dry overnight at room temperature. It was thought that there might be an effect of a faster and elevated temperature bake during processing that might affect the crystal structure of the PVDF, which could prevent beta phase formation [6]. By not

Table 4.3: PVDF Kynar resin and OMS suspended in DMAc

	Kynar (g)	OMS (g)	DMAc (mL)	OMS Weight %
PVOM.1	0.251	0	1	0
PVOM.2	0.364	0.014	1.5	0.65
PVOM.3	0.373	0.033	1.5	0.83
PVOM.4	0.504	0.015	2	1.89

baking out the solvent, it was ensured that the temperature exposure at that point was not a possible factor in a phase change.

4.2.1.4 Kynar Aquatec PVDF-based Paint with OMS

Kynar Aquatec, a PVDF-based latex paint, was obtained from Arkema in liquid form as described in Section 3.2.1.2. The formulation from Arkema was a 70/30 blend of PVDF and latex, respectively. As described in Chapter 3, the paint was combined with COTS additives to achieve a spray deposited uniform thin film that could be used in sensing applications and was applied to a substrate using a HVLP spray gun.

In order to investigate the possibility of developing a spray-deposited piezoelectric thin film based on a latex-based PVDF paint, varying amounts of OMS were added to a Kynar Aquatec based paint formulation. To make the Kynar Aquatec paint into a piezoelectric material it was thought that the addition of OMS could activate a phase change, similar to what was done by Buckley et al. [5]. Since the effect of sonication on the sample was not understood, four different samples were produced as shown in Table 4.4. (Note: the formulation for this paint is left out since the constituent concentrations are still considered proprietary at this point, however more than 50% of the formulation contains the Kynar Aquatec latex) The OMS powder in each of the mixed samples was the same at 0.23 % by weight.

4.2.2 Fourier Transform Infrared Spectroscopy

In order to determine if the phase of the PVDF was changed from alpha phase to beta phase, a FTIR microscope used. A Thermo Scientific Nicolet iN10 FT-IR microscope with a cooled mercury cadmium telluride (MCT) detector collected the spectra at liquid nitrogen temperatures. The spectra were typically collected at normal

Table 4.4: PVDF Aquatec mixture with OMS dispersed

	Mixing and sonication technique implemented
AquaOM.No	Lab Ram for 30 seconds at 40 % intensity with a speed of 60 Hz
AquaOM.A	Lab Ram for 30 seconds at 40 % intensity with a speed of 60 Hz, then ¼" ultra-tip-sonicated for 30 minutes with no pulse at 35 % amplitude
AquaOM.B	Lab Ram for 30 seconds at 40 % intensity with a speed of 60 Hz, then ¼" ultra-tip-sonicated for 6 minutes with no pulse at 35 %
AquaOM.C	Lab Ram for 30 seconds at 40 % intensity with a speed of 60 Hz, then placed in ice-water bath sonication for 1 hour

spectral resolution settings and using either 64 or 128 scans, depending upon the noise level. Since the spectra for PVDF lies in the mid-infrared region, the high spectral resolution capability of the iN10 microscope washed out any distinguishable and unique peaks for phase change characterization. The best spectra collection was observed when the attenuated total reflectance (ATR) fitting was used on the microscope. The signal filter used was a standard Beer-Norton, and there was no signal correction implemented during collection.

4.3 Results and Discussion

To evaluate the various effects of different weight percentages, chemical formulations, casting thickness, and drying conditions, a wide range of parameter variations were covered. FTIR was used to characterize the phase change transition of the final films produced and is provided for each combination studied for a thorough analysis of the phase change produced from each combination.

4.3.1 Kynar Resin Suspended in DMAc

Using the FTIR response, the structure of the PVDF thin film can be discerned from the other phases, which will allow for characterization of films fabricated with increasing amounts of DMAc. When the pure PVDF Kynar resin was suspended in DMAc solvent and baked out, the PVDF thin film was cast in the predominantly gamma phase. This is shown by a distinct peak at 1234 cm^{-1} rather than the alpha characteristic peak at 976 cm^{-1} or the beta characteristic peak at 1275 cm^{-1} in the FTIR spectra. In addition, from Figure 4.1, it appears that there is no concentration dependence of the amount of Kynar resin placed in the DMAc solvent, as once the DMAc solvent evaporates out completely, there is very little variation among the four FTIR spectra.

In addition, the qualitative appearance of these thin films was not very promising for use in sensing applications. It was found that with more Kynar resin in the solution, the film became more brittle. In addition, the more Kynar resin that was in the solution, the easier it was to detach it from the substrate. It is speculated that this could be due to the surface energy of the thin film and/or interfacial stress/strain due to the contraction of the film during drying. However, if there was not enough Kynar resin in the solution, the thin film would be very thin and clingy, yet still had very little elastic abilities. These thin films served as a solid basis for characterization of pure PVDF Kynar resin suspended in DMAc, but would not typically be used in sensing applications without additional additives to improve adhesion and elasticity.

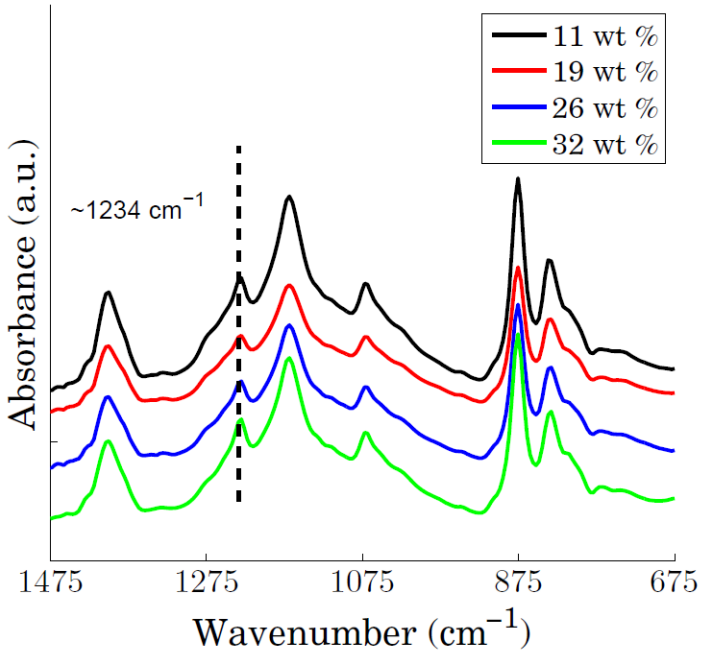

Figure 4.1: FTIR plot of various concentrations of PVDF Kynar resin suspended in DMAc solvent

4.3.1.1 Kynar Resin Suspended in DMAc Film Thickness Study

To evaluate if the issue of adhesion to the substrate and brittleness of the thin film was that only a drop was being dried out in the oven, a particular pipetted amount was placed on the aluminum substrate to investigate the effect of film thickness. In addition, the solvent evaporation rate would be much quicker in the thinner sample. The comparison of the FTIR spectra for the thick and thin samples is shown in Figure 4.2, which displays the same characteristic peaks for both samples.

Upon baking these samples, the 542.5 µm film appeared very brittle and detached from the aluminum substrate during heating. The adhesion of the film was very poor and would not serve well as a piezoelectric sensing film. The 77.5 µm film was better in terms of adhesion to the substrate since the contraction due to evaporation was much less than the thicker film. The 77.5 µm film did not detach upon baking until an attempt was made to attach the conductive tape for poling of the thin film. After the tape was attached to the film, it immediately pulled the film off of the aluminum substrate. Again, this film displayed poor adhesion properties and would not be a feasible piezoelectric paint for sensing applications.

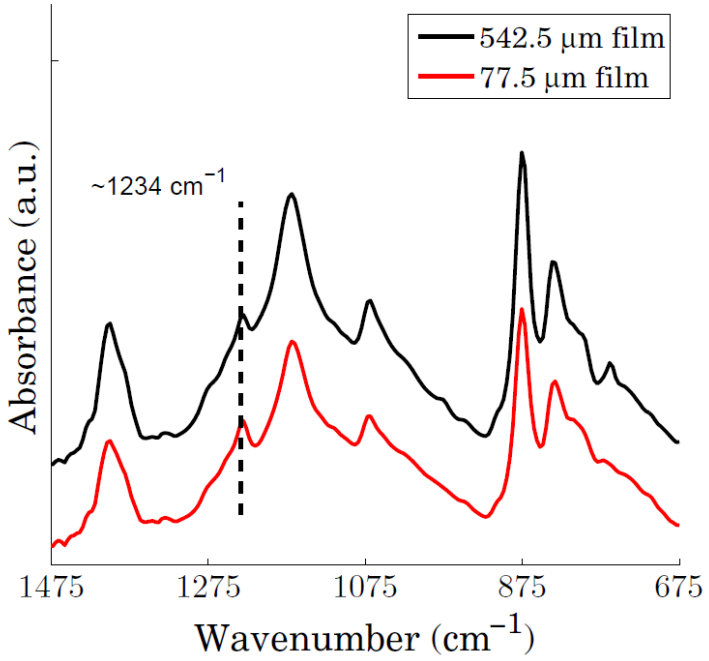

Figure 4.2: FTIR spectra to examine the effect of film thickness, and resulting solvent evaporation rate

4.3.2 Kynar Resin and OMS Suspended in DMAc

Once the effect of the addition of DMAc was characterized, the effect of the addition of OMS to films cast in DMAc was characterized using FTIR to determine if beta phase could be induced with this combination. To this end, four different weight percentages of OMS in a PVDF thin film were investigated, as stated in Section 4.2.1.3. The resulting FTIR spectra from these films are presented in Figure 4.3. Based on the gamma characteristic peak at 1234 cm^{-1}, it can be determined that the addition of OMS had no effect on the configuration of the PVDF in the thin films. This was unexpected as Buckley et al. [5], Cebe et al. [7], and Ince-Gunduz et al. [8, 9] all reported that concentrations as low as 0.025 % by weight showed a dominating beta phase. It is suspected that the chemical addition in these papers was not the determining factor in the phase change transition but rather the heat and pressure introduced during their specimen fabrication. Each author used some form of mechanical deformation in their processing (*i.e.* heat pressing or electrospraying) that played a larger role than discussed and emphasized in the phase change of the final samples.

The specimens that were dried overnight and were measured using FTIR 24 h after fabrication. The comparison of their spectra to that of the baked specimens can be seen in Figure 4.4. There appears to be no spectral variation between the samples that were dried in an oven at 70 ˚C for 1 h versus the samples that were dried

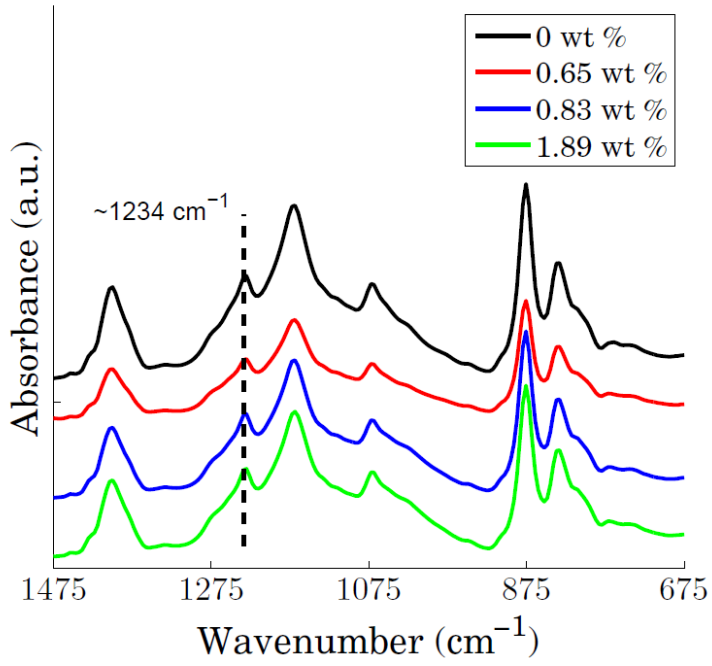

Figure 4.3: FTIR plot of various concentrations of PVDF Kynar and OMS suspended in DMAc solvent

overnight in a room at about 23 ˚C. This conclusion is different than that of Costa et al. [6] where the phase change present in the final sample was determined to be a byproduct of the different solvent evaporation rates.

The qualitative appearance of the baked and air-dried samples were very different. The baked films were opaque in color and did not have any particles present from the OMS from visual inspection as the air-dried films did. Thus, it was determined that OMS dispersion was good in these samples, yet, they still did not exhibit beta phase properties. In addition, these films had poor adhesion and became more brittle with increasing OMS content. The samples that were dried overnight at room temperature appeared white in color. The opaque appearance of these thin films was caused by the temperature and humidity conditions at which curing took place. Authors such as Li et al. [10] have performed studies that show the formation of the paraelectric alpha phase could appear opaque or transparent depending on the temperature and humidity during curing. Since the OMS was more of an off-white or cream color in powder form and not white as the thin films appeared after drying at room temperature, upon visual inspection it can be concluded that the OMS was dispersed and that the opaque appearance of the thin film was due to the membrane morphology of the alpha phase PVDF.

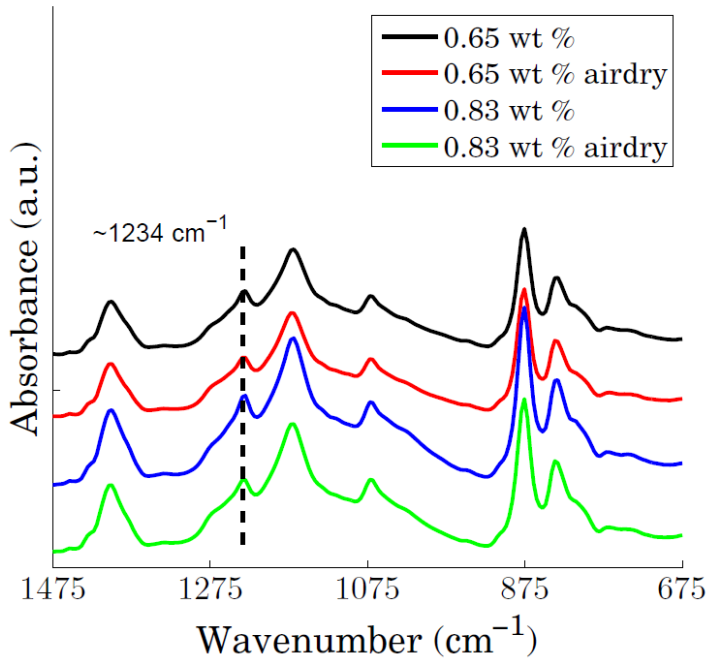

Figure 4.4: FTIR spectra to examine the effect of solvent evaporation rate

4.3.3 Kynar Aquatec PVDF-based Paint with OMS

Due to the excellent thin film properties of the Aquatec mixture, there were high hopes to induce a phase change in this solution. The addition of OMS was investigated by looking at a reference weight percent that should have activated a phase change according to Buckley et al. [5]. In addition, this small amount of OMS did not compromise the desirable film properties of the paint. Upon mixing, various sonication methods were investigated to evaluate proper dispersion of the OMS in the solution, since it was believed that the dispersion in the solution would be the key factor in forming a crystalline structure upon drying. The FTIR spectra from the four sonication methods are shown in Figure 4.5.

These films showed great adhesion and elasticity properties, as they were specifically designed for application to structures. Regardless of the sonication method used, there did seem to be small OMS particles that did not properly disperse. However, in regions where the agglomerations did not exist, it was plausible to collect the FTIR spectra. Unfortunately, as shown in Figure 4.5, the phase change did not occur as desired. Upon further investigation, since there were no changes observed from the addition of OMS, it was decided to try solely Kynar Aquatec in a DMAc solvent followed by heat treatment to evaporate the DMAc as was done with the pure PVDF Kynar resin. By doing so, it was examined if there was an observable phase change from alpha phase to

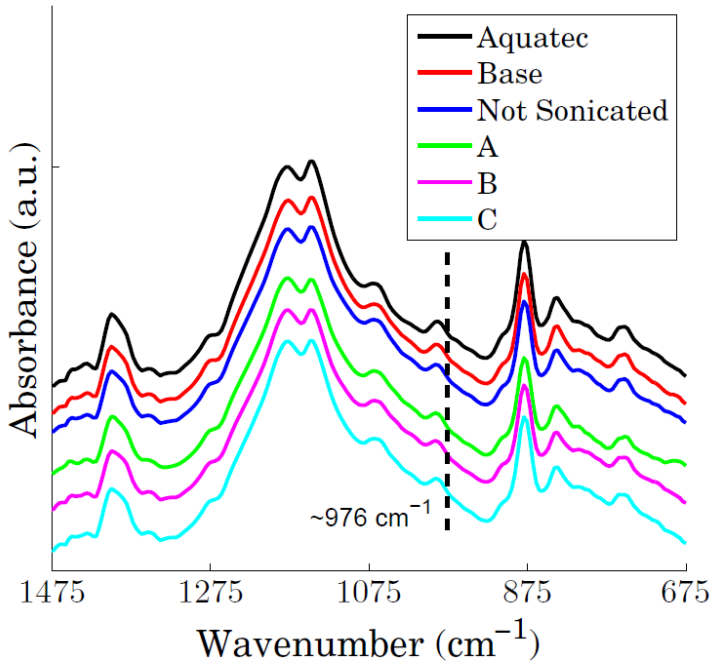

Figure 4.6: FTIR spectra to examine the addition of OMS and the effect of various sonication methods

gamma phase as was done with the pure PVDF. As shown in Figure 4.6, the phase change from alpha to gamma phase was not possible. This was most likely due to the fact that 30 % of the polymer content in the Kynar Aquatec

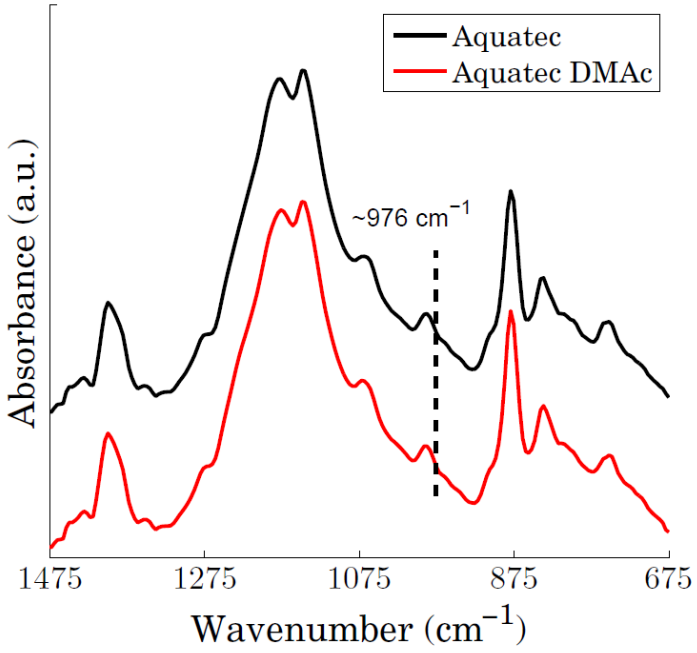

Figure 4.5: FTIR spectra to examine the effect of Aquatec suspended in a DMAc solution and then baked out

is a proprietary acrylate, which is to improve film quality. The Kynar Aquatec was designed to have low crystallinity for better elasticity, so even DMAc had little impact on creating a more crystalline structure.

4.4 Conclusions

The effect of DMAc and OMS induced phase change of PVDF thin films was concluded to not be very effective. Authors such as Buckley et al. [5], Cebe et al. [7], and Ince-Gunduz et al. [8] provided results that OMS could induce an alpha to beta phase change in PVDF thin films. Those results could not be reproduced here with PVDF-based paints nor pure PVDF suspended in DMAc as a solvent. After a closer review of the experimental procedure in the referenced papers, it was concluded that the chemicals were not the phase change activation method as reported but must be due to other fabrication factors, such as the compression molding at elevated temperatures as performed by Buckley et al. [5] and the electrospraying as performed by Costa et al. [6]. A compression molding step would mechanically work the thin films and induce a phase change similar to mechanically working a liquid suspension by generating surface tension during electrospraying. It was concluded that the phase change of PVDF cannot be achieved solely through chemical formulation; but rather, the sample preparation process must still incorporate some form of mechanical stretching.

Chapter 4 References:

1. Kim, G.H., S.M. Hong, and Y. Seo, *Piezoelectric properties of poly(vinylidene fluoride) and carbon nanotube blends: beta-phase development.* Physical Chemistry Chemical Physics, 2009. **11**: p. 10506-10512.
2. Huang, W., et al., *Nanocomposites of Poly(vinylidene fluoride) with Multiwalled Carbon Nanotubes.* Journal of Applied Polymer Science, 2009. **115**: p. 3238-3248.
3. Ploss, B., et al., *Poling study of PZT/P(VDF-TrFE) composites.* Composites Science and Technology, 2001. **61**: p. 957-962.
4. Chan, H.L.W., P.K.L. Ng, and C.L. Choy, *Effect of poling procedure on the properties of lead zirconate titanate/vinylidene fluoride-trifluoroethylene composites.* Applied Physics Letters, 1999. **74**(20): p. 3029-3031.
5. Buckley, J., et al., *Nanocomposites of poly(vinylidene fluoride) with organically modified silicate.* Polymer Science Direct, 2006. **47**: p. 2411-2422.
6. Costa, L.M.M., R.E.S. Bretas, and R.G. Jr., *Effect of Solution Concentration on the Electrospray/Electrospinning Transition and on the Crystalline Phase of PVDF* Materials Sciences and Applications, 2010. **1**: p. 247-252.
7. Cebe, P. and J. Runt, *P(VDF-TrFE)-layered silicate nanocomposites. Part 1. X-ray scattering and thermal analysis studies.* Polymer Science Direct, 2004. **45**: p. 1923-1932.
8. Ince-Gunduz, B.S., et al., *Impact of Nanosilicates on poly(vinylidene fluoride) crystal polymorphism: Part 1. Melt-crystallization at high supercooling.* Polymer Science Direct, 2010. **51**: p. 1485-1493.
9. Ince-Gunduz, B.S., et al., *Impact of Nanosilicates on Poly(vinylidene fluoride) Crystal Polymorphism: Part 2. Melt-crystallization at Low Supercooling.* Journal of Macromolecular Science, Part A: Pure and Applied Chemistry, 2010. **47**: p. 1208-1219.
10. Li, M., et al., *Controlling the microstructure of poly(vinylidene-fluoride) (PVDF) thin films for microelectronics.* Journal of Materials Chemistry C: Materials for optical and electronic devices, 2013. **1**(46): p. 7695-7702.

Chapter 5: Conclusions

The work performed and described in this thesis has benefitted the discipline focused on the use of PVDF in structural health monitoring applications by examining the methodology of phase change in PVDF to transition from the non-polar non-piezoelectric alpha phase to a polarized, piezoelectric beta phase. This thesis provides a thorough examination into current phase change activation methods and evaluates existing recommendations based on current literature. The description of this work was designed to illustrate the major issues that are presented in current literature recommendations of inducing a phase change in PVDF-based sensing films and provides a recommendation on what truly needs to be performed to exploit the piezoelectric sensing capabilities of PVDF and PVDF-based sensing thin films in impact damage detection systems.

The work performed in Chapter 2 was solely based on research focusing on the *in situ* characterization of mechanically stretched PVDF-based thin films to convert alpha phase PVDF to the polarizable form of beta phase PVDF. From the discussion presented, the gradual transition from the distinct alpha peak at 794 cm^{-1} to the distinct beta peak at 839 cm^{-1} using Raman spectroscopy confirmed that the transition is not a sudden change but rather an evolving one based on the stretch ratio in the material. In addition, the phase change transition of alpha to beta phase PVDF produced from mechanical stretching was confirmed. Lastly, the confirmed stretch ratio of only 1.5 was concluded to be all that was necessary to succeed in a phase change which, is much lower than that of previous literature. Due to the inability of scaling this phase change transition to large-scale complex geometry structures, the continuing research of this thesis examined methods that could scale up.

The work performed in Chapter 3 focused on the concurrent use of high voltage and high temperature applied to a pure PVDF thin film as well as a PVDF-based latex paint. Due to the limitations on voltage, the pure PVDF thin film was not able to exhibit any phase changes as the voltage applied was just not large enough. For the PVDF-based latex paint, there were issues of dielectric breakdown that prevented any success in achieving a phase change transition. When high voltages were applied at high temperatures, the material experienced a dielectric breakdown at low voltages where there was no observation of phase transition. To be able to handle the higher

voltages poling had to take place at room temperature. This prevented a phase change transition as well. The concurrent application of high voltage and high temperature proved to be unsuccessful for the purpose of this thesis.

The work performed in Chapter 4 focused on the phase change transition of PVDF-based paints stemming from the addition of chemical additives such as dimethyl acetamide and organically modified silicate. Literature papers referenced in this chapter claimed that a simple addition of OMS could induce a phase change. However, this conclusion was not reproducible and is shown by adding OMS to a PVDF mixture in various concentrations and using FTIR to evaluate the phase present. The alpha to beta phase transition was unobservable. In addition, it was found that when pure PVDF Kynar resin was mixed in dimethyl acetamide and the solvent was baked, the gamma phase was produced.

In conclusion, this work has further enabled research into PVDF and PVDF-based paints to be used in sensing applications, particularly for impact damage detection in large-scale complex geometry systems, by identifying the methods to phase change PVDF that can actually produce a scalable thin film. It was found that phase change transition from alpha phase to the more useful beta phase was very difficult without some form of mechanical stretching of the material. The necessity of mechanical stretching may reduce the desirability of pure PVDF thin films for large scale applications, as they must be mechanically deformed prior to application to any large-scale complex geometry system. Future work should look to methods that implement some form of mechanical stretching in addition to the application of concurrent high voltage and high temperature and/or chemical additives to induce a phase change.